https://doi.org/10.5194/egusphere-2025-3713
Preprint. Discussion started: 27 August 2025

Substantial inter-model variation in OAE efficiency between the CESM2/MARBL and ECCO-Darwin ocean biogeochemistry models

Michael D. Tyka[1], Mengyang Zhou[2,3], Elizabeth Yankovsky[2,3,4], and Dustin Carroll[5,6]

[1]Google Inc., Seattle, WA 98103, USA
[2]Department of Earth and Planetary Sciences, Yale University, New Haven, CT 06511, USA
[3]Yale Center for Natural Carbon Capture, New Haven, CT 06511, USA
[4][C]Worthy, LLC, Boulder, CO 80302, USA
[5]Moss Landing Marine Laboratories, San José State University, Moss Landing, CA 95039, USA
[6]Jet Propulsion Laboratory, California Institute of Technology, La Cañada Flintridge, CA 91011, USA

Correspondence: Michael D. Tyka (mike.tyka@gmail.com)

Abstract. Induction of a surface-ocean DIC (dissolved organic carbon) deficit through alkalinity-based or direct CO_2 removal methods has been recognized as a promising approach to meet the projected need for negative emissions. The difficulty of directly measuring the counter-factual CO_2 flux due to rapid spreading of the DIC-deficient plume has put ocean circulation models in the center of the Measurement, Reporting and Verification (MRV) challenge. Confidence in the results of such models is essential for the emerging industry to access carbon credit markets and grow at the required pace, to reach substantial negative emissions by 2050, as envisioned by the Intergovernmental Panel on Climate Change (IPCC).

The kinetics and equilibration time of such a DIC deficit have been shown to vary substantially depending on the location and season of the initial induction point. A major component of this variance is the vertical transport and mixing of the DIC-deficient plume; however, air-sea CO_2 gas exchange and carbonate chemistry are also important.

Currently, it is poorly understood how much the results of DIC-deficit pulse simulations depend on the models chosen. To help close this knowledge gap, we investigate two global circulation models, the CESM2/MARBL model (1°) and the data-assimilative ECCO-Darwin model (1/3°). We perform pulse injection simulations at twelve locations with both models, matched precisely in terms of injection patch geometry, release year and season. We analyze the differences in CO_2 uptake curves, vertical mixing, gas exchange and carbonate chemistry.

We show that in some locations, such as subtropical regions, substantial differences exist between these two models — well beyond the expected intrinsic variation of each model. Furthermore, we demonstrate that the majority of the differences are attributable to the representation of vertical transport, followed by the effect of wind parameterizations. A small amount of difference is attributable to carbonate chemistry parameterization. In some locations, there exists good agreement between the models. In most injection locations, the largest differences between models are found in the first 7 years post alkalinity injection, followed by slow convergence towards the expected theoretical maximums.

https://doi.org/10.5194/egusphere-2025-3713
Preprint. Discussion started: 27 August 2025

1 Introduction

Marine Carbon Dioxide Removal (mCDR) methods (Press, 2022; Oschlies et al., 2023; Renforth and Henderson, 2017) have recently gained significant attention as a scalable set of approaches to achieve the magnitude of negative emissions called for by IPCC models to keep global-mean temperatures below 2°C by 2100 (Rogelj et al., 2018; Metz and Intergovernmental Panel on Climate Change, 2005; Masson-Delmotte et al., 2021; Rickels et al., 2018). These methods work by inducing a pCO_2 deficit in the surface ocean, which causes excess CO_2 uptake by the ocean. The word excess here is used to indicate the excess relative to a counterfactual scenario without the intervention. The pCO_2 deficit can be created in a variety of ways. The removal of CO_2 from surface waters (Direct Ocean Removal, DOR) and subsequent storage of CO_2 in geological reservoirs or the cultivation of macroalgae followed by removal or sinking of plant matter both remove dissolved inorganic carbon (DIC) from surface waters. Alternatively, the dissolution of alkaline materials in surface water or the removal of acidity through electrochemical means also lead to a DIC deficit by altering the carbonate equilibrium (Oschlies et al., 2023; Renforth and Henderson, 2017).

In both situations, however, the induction of the pCO_2 deficit does not immediately remove CO_2 from the atmosphere (Broecker and Peng, 1982). Instead, this process occurs on the order of years or decades, depending on the speed of gas exchange and the residence time of surface waters (Jones et al., 2014; Wang et al., 2023; Suselj et al., 2025). Previous work has shown a complex dependency on the release location as the DIC deficient plume spreads over entire ocean basins on the timescale of equilibration, with subduction processes removing the deficit from contact with atmosphere while also transporting it later into surface waters elsewhere (He and Tyka, 2023; Suselj et al., 2025; Zhou et al., 2024).

The geographical region over which ocean dynamics contribute to the equilibration process is so large that direct experimental measurement of the counterfactual CO_2 uptake is extremely difficult in practice (Mace et al., 2021; Subhas et al., 2025) considering that the dilution of the plume leads to sub-μM changes in surface pCO_2 (He and Tyka, 2023), which are very difficult to measure (Wanninkhof et al., 2013). Furthermore, the counterfactual values of surface pCO_2 are inaccessible to direct measurement and changes in pCO_2 are difficult to attribute if multiple OAE deployments overlap in their alkalinity plumes He and Tyka (2023). Therefore, the Measurement, Reporting and Verification (MRV) of mCDR efforts will likely lean very heavily on ocean modelling (Bach et al., 2023; Fennel et al., 2023).

Recently, an extensive map of Ocean Alkalinity Enhancement (OAE) equilibration curves, covering multiple seasons, was calculated using the CESM2/MARBL general circulation model (GCM) (Zhou et al., 2024) and strong seasonal and regional differences were identified. Yankovsky et al. (2025) extended the work to investigate interannual variability, which is inherent to any given model, and found some regions exhibit substantial variation of uptake rates from year to year, owing to differences in flow patterns. However, to date, the inherent model uncertainty or confidence relative to other models is largely unknown. Previous efforts have compared different circulation or Earth System Models (ESMs) and the variance in their predictions (Keller et al., 2018), but specifically how their differences influence the OAE equilibration curves has not been explored. Xie et al. (2025) recently investigated the effect of different horizontal grid resolutions and found comparatively small differences across different resolutions of the same model, noting that the resolutions spanned 0.1° to 1° and at best only resolved the mesoscales, but large differences comparing entirely different models to each other. We therefore focus our attention to

https://doi.org/10.5194/egusphere-2025-3713
Preprint. Discussion started: 27 August 2025

comparing two models side-by-side (the aforementioned CESM2/MARBL GCM and the ECCO-Darwin model) using pulse injections of alkalinity. Our goal is to examine not only the extent of the variability but to pinpoint the components of the model set-ups or parameterizations which make the largest difference to the equilibration curves.

2 Methods

2.1 Ocean models

Using the polygonal subdivision of the ocean introduced in Zhou et al. (2024), we selected 12 locations, spanning the range of the four different OAE uptake regimes identified by Zhou et al. (2024). The locations chosen are shown in Fig. S1 and listed in Table S1. Since the ECCO-Darwin model uses a different grid (LLC270 grid at 1/3° (Zhang et al., 2018)) compared to the CESM2/MARBLE model (1° spherical-polar grid), we re-projected the polygonal subdivisions (Zhou et al., 2024) onto the finer, 1/3° LLC270 grid. While the difference in gridding means that the release locations cannot be exactly replicated, the difference in the release area boundary is very small and not expected to significantly alter the uptake curves. This assumption is supported by the observation that the $\eta(t)$ curves obtained previously vary across the ocean only gradually (Zhou et al., 2024). In each location, alkalinity was released over the period of one month (in January) at a rate of 5 mol m^{-2} yr^{-1} uniformly across the selected polygon.

We conducted each of the pulsed alkalinity simulations using the standard LLC270 ECCO-Darwin 1/3° model setup for 15 years (Zhang et al., 2018; Carroll et al., 2020, 2022, 2024). For each location, we investigated two pulses, one in 1992 and one in 1999 in two separate simulations. The latter matches the exact release year used in Zhou et al. (2024) while the former provides an indication of the interannual variability. The atmospheric concentration of CO_2 was set to historical values from the NOAA Greenhouse Gas Marine Boundary Layer Reference(Andrews et al., 2014). Small differences in pCO_2^{atm} are not expected to change the OAE uptake curves, so long as the value is not responsive to induced CO_2 uptake (Tyka, 2025). The total volume-integrated amount of ocean DIC was then computed over the simulation period and the difference to a reference simulation was obtained. This was then normalized by the total amount of alkalinity added initially to give $\eta(t) = \Delta\Sigma DIC(t)/\Delta\Sigma Alk$ as the metric of OAE efficiency (Zhou et al., 2024), where the sums are over the entire ocean volume.

In the same way as described above, we also tested four additional locations (North Pacific, North Hawai'i, Equatorial Pacific and Gulf Stream) replicating exactly the experiments of Yankovsky et al. (2025). Here, 5 runs were conducted for 5 years each, with alkalinity addition pulses in January of 2000, 2003, 2006, 2009 and 2012, with the goal of quantifying interannual variability.

2.2 CESM2/MARBL

The CESM2/MARBL model configuration used in this study is described in detail in Zhou et al. (2024) and references therein. Briefly, the CESM2/MARBL simulation is a global forced ocean-ice (FOSI) configuration (Yeager et al., 2022) of the Community Earth System Model v.2 (CESM2) (Danabasoglu et al., 2020). The ocean component is the Parallel Ocean Program

https://doi.org/10.5194/egusphere-2025-3713
Preprint. Discussion started: 27 August 2025

v.2 (POP2) with nominal horizontal resolution of 1° × 1° and biogeochemistry simulated by MARBL (Long et al., 2021). The model was forced with the Japanese 55-year atmospheric reanalysis dataset (JRA55) (Kobayashi et al., 2015), spun up from 1850 to 2019. All simulations in this study were forced with historical atmospheric CO_2. Further properties and features of the model are summarized in Table 1.

2.3 ECCO-Darwin

A detailed description of the ECCO-Darwin model setup, observational constraints, optimization methodology, and model-data evaluation is presented in Carroll et al. (2020, 2022, 2024). The latest ECCO-Darwin solution (v05) used here is based on ocean circulation and physical tracers (i.e., temperature, salinity, and sea ice) from the Estimating the Circulation and Climate of the Ocean (ECCO) LLC270 global-ocean and sea-ice data synthesis (Zhang et al., 2018). ECCO-Darwin is based on a global-ocean and sea-ice configuration of the Massachusetts Institute of Technology general circulation model (MITgcm) (Marshall et al., 1997), which has been constrained by the ECCO project using nearly all available ocean observations for the 1992–near-present period and has horizontal grid spacing of 1/3° at the equator and ∼18 km at high latitudes, with 50 vertical levels. The ECCO circulation estimate is coupled with the MIT Darwin ocean ecosystem model, which in turn drives and interacts with marine chemistry and ocean carbon variables (Dutkiewicz et al., 2015), providing a data-constrained, property-conserving estimate of the three-dimensional, time-evolving ocean, sea ice, biogeochemical, and ecological state. An extensive global-ocean evaluation of ECCO-Darwin against in-situ data is provided in Carroll et al. (2024).

Table 1 summarizes the main features and parameterizations for both models.

2.4 Overall inter-model differences

In addition to quantifying the empirical differences in OAE-induced CO_2 uptake between different ocean circulation models, the goal of this paper is to estimate the relative importance of different model aspects to the overall variance. A better understanding of these sources of discrepancy will inform future model development and potentially inspire new sources of model-constraining data collection.

The main aspects of the ocean models which conceivably contribute to the CO_2 equilibration dynamics are: horizontal and vertical transport (advection and mixing) of the excess alkalinity plume, the gas transfer velocities (which are a function of wind speed), the carbonate chemistry parameterization and any biological processes which can affect DIC or alkalinity concentration. These aspects are strongly intertwined; for example, changes in horizontal transport will affect plume dispersal and therefore which gas transfer velocities will be encountered by the space-time evolving trajectory of the plume.

We first compare these aspects in a generic way, comparing the wind forcing and carbonate parameters as function of latitude, longitude and time. These comparisons help identify overall differences in parameterization and are not specific to any given injection location. We then conduct a deeper analysis which compares the influence of each parameter to any given release location and alkalinity plume.

https://doi.org/10.5194/egusphere-2025-3713
Preprint. Discussion started: 27 August 2025

Feature	CESM2/MARBL	ECCO-Darwin
Type	Hand-tuned hindcast simulation	Data-assimilative hindcast simulation
Optimization	Atmospheric and sea ice tuning to help balance the radiative budget. Langmuir mixing parameterization in conjunction with the wave model component Estuary mixing parameterization. Increased mesoscale eddy diffusivities at depth.	Adjoint methods for physics, Green's Functions approach for biogeochemistry. Adjusted: initial conditions, surface-ocean boundary conditions, and time-invariant, 3-D mixing coefficients.
Grid	Spherical-polar, nominal 1° x 1°. Uniform zonal resolution of 1.125° and varying meridional resolution (29–72 km) from 0.27° (equator) to 0.64° (northwestern Pacific Ocean)	Lat-Lon-Cap (LLC), Nominal 0.33° x 0.33° (37 km at the equator, ∼18 km at high latitudes)
Vertical levels	60 levels (10–250 m)	50 levels (10–456.50 m)
Advection	Third-order upwind scheme	Third-order upwind (horizontal) and third-order direct-space-time (vertical)
Vertical diffusion	K-Profile Parameterization vertical mixing (Large et al., 1994) with depth-dependent, time-invariant 3-D background diffusivity.	Gaspar et al. (1990) vertical mixing with time-invariant, 3-D background diffusivity that is optimized using the adjoint method.
Horizontal diffusion	Smagorinsky-like formulation for anisotropic horizontal viscosity. Gent-McWilliams (GM) isopycnal diffusion for tracers to represent mesoscale eddy impact. Explicit sub-mesoscale mixing enabled. GM diffusivity is 3.0x10^3 m^2/s at surface boundary layer and 0 at bottom.	Gent-McWilliams and Redi (GM-Redi) isopycnal diffusion for tracers, representing mesoscale eddy impact on large-scale ocean circulation. The 3-D parameters of GM-Redi are optimized via the adjoint method.
Atmospheric wind forcing	3-hourly JRA55 (1958-2018)	6-hourly ERA Interim with adjoint-method-based 14-day atmospheric corrections.
Ice coverage	Sea-ice simulated prognostically using the CICE model, version 5.1.2 (CICE5, eight vertical layers) (Yeager et al., 2022).	MITgcm sea ice model, viscous-plastic rheology on a C-grid, zero-layer thermodynamics, optimized via SST adjustment.
Riverine forcing	JRA55 (1958-2018)	Smoothed monthly-mean river discharge climatology (Fekete et al., 2002).
Air-Sea gas exchange	k = $0.251u^2$(Sc/660)$^{-1/2}$, (Wanninkhof, 2014).	k=$0.337u^2$(Sc/660)$^{-1/2}$, (Wanninkhof, 1992), modified based on OCMIP results (Dietze and Oschlies, 2005).
Atmospheric pCO_2	Historical (1850–2014) and SSP3-7.0 (2015–2100) atmospheric pCO_2 (Eyring et al., 2016)	NOAA MBL (Andrews et al., 2014)
Tracers	Alk, DIC + 30 other biogeochem. tracers (Long et al., 2021)	Alk, DIC + 29 other biogeochem. tracers (Darwin)
Phytoplankton model	3 explicit phytoplankton types (diatoms, diazotrophs, small pico/nano phytoplankton), 1 implicit type (calcifiers), and 1 zooplankton type. Long et al. (2021)	5 phytoplankton types (diatoms, other large eukaryotes, Synechococcus, low- and high-light adapted Prochlorococcus) and two zooplankton types.
References	Zhou et al. (2024), Yeager et al. (2022)	Carroll et al. (2020), Zhang et al. (2018), Forget et al. (2015)

Table 1. Side by side comparison of the two biogeochemical models used in this study.

https://doi.org/10.5194/egusphere-2025-3713
Preprint. Discussion started: 27 August 2025

2.4.1 Carbonate parameters

As a further reference point we also compared both models' carbonate parameters to a data-based product. Experimental data for global surface-ocean alkalinity (Alk), DIC and pCO_2 were obtained from OceanSODA (Gregor and Gruber, 2021). The simulations with CESM2/MARBL and ECCO-Darwin also generated monthly-mean $[Alk]$ and $[DIC]$ fields throughout the simulation. For analysis and comparison purposes, the data from ECCO-Darwin and OceanSODA were regridded onto the OceanSODA grid, using nearest neighbor interpolation. For the latitudinal comparison of carbonate parameters (Fig. 6) the Mediterranean Sea was excluded. Based on values of surface-ocean $[Alk]$ and $[DIC]$, as well as salinity, temperature and concentrations of borate, phosphate and silica, the full carbonate system was solved on the surface using PyCO2SYS (Humphreys et al., 2020) at monthly intervals, yielding values for $[CO_2]$, $[HCO_3^-]$ and $[CO_3^{2-}]$. The quantity $\eta_{max} = \partial[DIC]/\partial[Alk]$ was calculated using the exact equation (for derivation see Supplement and Humphreys et al. (2018))

$$\frac{\partial[DIC]}{\partial[Alk]} = \frac{[HCO_3^-] + 2[CO_3^{2-}]}{[HCO_3^-] + 4[CO_3^{2-}] + [OH^-] + [H^+]) + [B(OH)_4^-][B(OH)_3]/B_T} \tag{1}$$

where B_T is the total borate concentration. The carbonate sensitivity $\partial[DIC]/\partial[CO_2]$ was, likewise, calculated using an exact equation (for derivation see Supplement):

$$\frac{\partial[DIC]}{\partial[CO_2]} = \frac{[DIC]}{[CO_2]} - \frac{([HCO_3^-] + 2[CO_3^{2-}])}{[CO_2]} \frac{\partial[DIC]}{\partial[Alk]}. \tag{2}$$

2.5 Ablation of biological model

Another way to compare models is to conduct what is known in the machine learning community as "ablation". Here, parts of a model are deliberately turned off or changed, and the simulations are repeated to examine their effects on the outcomes. We take this approach here with the biogeochemical model of ECCO-Darwin, which comprises 31 biogeochemical tracers, which, in addition to Alk and DIC, include Oxygen, Nitrate, Nitrite, Ammonia, Phosphate, Iron, Silica, Dissolved Organic Carbon and multiple phytoplankton functional type tracers among others. These tracers are used to simulate biological activity, nutrient dynamics and carbonate precipitation and dissolution, in addition to inorganic processes such as gas exchange. Since these processes can consume or produce CO_2, while in principle also being rate-dependent on the state of the carbonate chemistry, it is conceivable that they influence gas exchange and OAE equilibration.

We thus created an ablated version of the ECCO-Darwin in which the marine ecosystem component was turned off in the code, i.e. an ocean without the soft tissue pump or calcifying activity. The only processes that remained active were the surface gas exchange, the advection of the tracers Alk and DIC, and the calculation of the carbonate system and pH. Alkalinity injections in eight different locations (plus an unperturbed reference run) were examined in this way, each with one run conducted with, and one run conducted without biological processes enabled. Note that we did not spin up the system anew, or let the system reequilibrate into a new steady state which lacks the soft tissue pump and its associated DIC gradients before running the simulations. This was done intentionally to avoid changing the background carbonate state of the surface ocean, which would undoubtedly change the uptake kinetics. Instead, this experiment asks more narrowly: does the simulation

https://doi.org/10.5194/egusphere-2025-3713
Preprint. Discussion started: 27 August 2025

of biological processes directly influence the CO_2 uptake curves on a short timescale (15 years)? The sudden loss of the biological pump at the beginning of the simulations of course causes a steady departure of DIC from the regular ECCO-Darwin trajectory; however those changes are still relatively small over the 15-year model period, such that the background ocean state still corresponds well to the full ECCO carbonate state.

2.6 Plume-specific intermodel differences

In addition to determining the overall differences and variance in CO_2 uptake kinetics between the two models, it would be valuable to understand which parameterization differences contribute the most to these differences. Two major processes conceivably affect the CO_2 equilibration dynamics: Firstly, the parameterization of gas transfer (i.e., wind speeds, gas-exchange, carbonate chemistry parameters and biological model) directly affect the equilibration process. Secondly, the trajectory of the plume determines the surface-ocean dilution (since only alkalinity in contact with the atmosphere contributes to gas exchange) and the horizontal trajectory, which determines which gas exchange conditions the plume will encounter at the surface.

In theory, one could repeat each set of simulations, while replacing just one aspect at a time, effectively morphing one model into the other, step by step, noting which substitutions contribute the most to recapitulating the CO_2 uptake curve of the other model. However, this comes at a high computational price and would be infeasible for expensive, high resolution models.

Instead, we take a different approach, whereby the effective equilibration rate constant is "reconstructed" from its component terms offline, which include the surface dilution, surface distribution of the plume and the gas-exchange and carbonate parameters, as detailed below. In this framework one can then directly examine the sensitivity with respect to any given parameter.

2.6.1 Effective rate constant of equilibration

Addition of alkalinity to seawater shifts the carbonate equilibrium towards carbonate and away from CO_2, thereby reducing its partial pressure pCO_2, increasing its pH and causing additional uptake of CO_2 from the atmosphere.

If allowed to fully re-equilibrate with the atmosphere (not accounting for reservoir feedbacks (Tyka, 2025)) the addition of a small quantity $\Delta[Alk]$ will eventually increase the total DIC of the water parcel by $\Delta[DIC]_{eq}$:

$$\Delta[DIC]_{eq} = \Delta[Alk] \left.\frac{\partial[DIC]}{\partial[Alk]}\right|_{pCO_2} \tag{3}$$

where the partial derivative $\eta_{max} = \partial[DIC]/\partial[Alk]$ is taken at constant pCO_2.

After alkalinity is introduced to the surface ocean, but before full equilibration is complete, there is therefore effectively a deficit in $[DIC]$ relative to its final equilibrated state, termed $[D](t)$, which varies with time t.

$$[D](t) = \Delta[DIC]_{eq} - \Delta[DIC](t) \tag{4}$$

As time evolves, the ocean absorbs additional CO_2 from the atmosphere, which reduces the remaining DIC deficit $[D](t)$ and the surface pCO_2 difference between the perturbed and reference simulation. For the ocean models examined in this paper,

https://doi.org/10.5194/egusphere-2025-3713
Preprint. Discussion started: 27 August 2025

the CO_2 gas exchange parameterization assumes that the flux of CO_2 across the air-sea interface, F_{CO_2}, is proportional to the partial pressure difference:

$$F_{CO_2} = k\alpha(pCO_2^{atm} - pCO_2^{ocn}), \tag{5}$$

where α is the solubility of CO_2 in seawater (mol m^{-3} atm^{-1}) and k is the effective gas transfer velocity (m s^{-1}). Typically, k is parameterized as a function of wind speed squared $k_w \propto U^2$ (Ho et al., 2006; Wanninkhof, 2014) and weighted by the sea-ice cover fraction α_{ice}, where it is assumed that complete sea-ice cover fully suppresses air-sea gas exchange.

$$k = (1 - \alpha_{\text{ice}})k_w \tag{6}$$

This leads to the following differential equation describing the equilibration of any induced DIC deficit $[D](t)$ over time (Zeebe and Wolf-Gladrow, 2001; Zhou et al., 2024):

$$\frac{\mathrm{d}}{\mathrm{d}t}[D] = -\frac{k}{\beta}\frac{\mu}{z_0}[D], \tag{7}$$

where μ is the surface-ocean dilution factor, i.e., the fraction of the DIC deficit in the exchanging surface grid cells of the model, of depth z_0. The factor $\beta = \frac{\partial[\mathrm{DIC}]}{\partial[CO_2]}$ accounts for the fact that the effective capacity of the ocean for CO_2 is vastly increased due to the fast carbonate equilibrium with bicarbonate and carbonate ions and depends on the local carbonate system state and varies over the global ocean; a typical value is around 10–20 (Zeebe and Wolf-Gladrow, 2001). This coupling (which is absent for other gases) significantly increases the equilibration time of CO_2. Taken together, the overall effective rate constant for this first order equilibration is $r = \frac{k}{\beta}\frac{\mu}{z_0}$.

Since in the simulations examined here the excess alkalinity is not added uniformly but at a single polygon location, the equilibration process is spatially confined to the extent of the plume. As the plume spreads, the parameters determining the rate constant will change, and they potentially change differently in different models.

To create a framework in which to quantify the localized impact of parameter differences on the overall equilibration process, we make the reasonable assumption that the total deficit equilibration rate $\frac{\mathrm{d}}{\mathrm{d}t}[D]$ can be expressed as a sum over all the contributing surface-ocean grid cells:

$$\frac{\mathrm{d}}{\mathrm{d}t}[D] = \sum_{ij} -\frac{k_{ij}\mu_{ij}}{\beta_{ij}z_0}w_{ij}[D], \tag{8}$$

where the variables i and j sum over the surface grid and w_{ij} weights the contribution of any particular surface-ocean grid cell to the overall equilibration process, such that that total sum of weights equals one: ($\sum_{ij} w_{ij} = 1$). Note that the surface-ocean parameters k_{ij} and β_{ij} depend on latitude, longitude and time but are independent of the injection plume or its location.

https://doi.org/10.5194/egusphere-2025-3713
Preprint. Discussion started: 27 August 2025

In contrast, μ_{ij} and w_{ij} are dependent on latitude, longitude and time as well as the spatial distribution of the particular spreading alkalinity plume. Written as above, one can consider the expression of the overall effective rate constant r as being:

$$r = z_0 \sum_{ij} \frac{k_{ij}}{\beta_{ij}} \mu_{ij} w_{ij} \tag{9}$$

Ideally, the weights w_{ij} would be based directly on the remaining deficit $[D]$ in each surface cell, calculated by Eq. 3 and 4. However, a conceptual problem with using the deficit for the spatial weighting is that the remaining deficit and its distribution depend on the gas exchange itself up to that point in time. Therefore, using it to estimate the rate constant does not cleanly factor the effects of plume trajectory and gas exchange. For example, when estimating the effect of changing the gas-exchange parameterization while keeping the plume trajectory constant, representing the trajectory by the deficit from a given simulation leaks some of the gas exchange behavior from that simulation into the comparison. An additional issue we found with using the deficit for weighting, is that it numerically unstable when calculating ratios between rate constants from two different simulations (see below), because the values of $[D]$ can become extremely small. This is because it naturally tends towards zero as the equilibration proceeds, and can even become slightly negative (due to processes other than equilibration changing [Alk], [DIC] and $\partial[Alk]/\partial[DIC]$ in the Lagrangian frame of the plume).

A more practical way to assign weights to the alkalinity plume is to set them to the fraction of total excess alkalinity (equilibrated and unequilibrated) contained in any given location. Unlike the deficit, the excess alkalinity represents an essentially conservative tracer which maps out the transport of the plume, unaffected by gas exchange. Here, w_{ij} captures the horizontal trajectory of the plume while μ_{ij} captures the vertical dilution of the plume. The product $\mu_{ij} w_{ij}$ is equal to the fraction of the total alkalinity currently resident in the surface cell (i, j). The disadvantage is that the spatial alkalinity distribution does not exactly mirror the distribution of the deficit, such that the weighting should be considered approximate.

2.7 Comparing the rate constant from two different simulations

Using this framework, we wish to gain insight into the relative contributions of the above parameters on the overall gas exchange rate. In other words, given a particular plume trajectory, how much does the choice of parameter set k or β change the rate constant of the overall equilibration process? Conversely, given a particular parameter set, how much does the trajectory of the plume change the rate of equilibration?

To answer these questions, we define a simple metric which compares the estimated equilibration rate constant r from two simulations A and B into a single quotient Q.

$$Q = \frac{r^A}{r^B} \tag{10}$$

If $log(Q)$ is greater than 0 then the equilibration is faster in simulation A, else it is faster in simulation B. Note the Q varies over time, as the parameters and the plume are both time-dependent properties (i.e. $Q(t) = r^A(t)/r^B(t)$). This approach is appealing because it expresses the differences in the equilibration rate constant in a unitless, relative way. As such, however, Q does not resolve which contributors to r^A or r^B are responsible for the majority of the differences.

https://doi.org/10.5194/egusphere-2025-3713
Preprint. Discussion started: 27 August 2025

2.7.1 Differences due to the different k and β parameterizations.

To extract this information we define a set of different metrics where all the terms are set equal except for one parameter, which is singled out for comparison. That one parameter is taken from model A in the numerator of the quotient Q and from model B in the denominator of the quotient Q. The ratio of the resulting rate constants then gives a measure of how much the equilibration rate is influenced by swapping out a particular parameter.

For example, consider the expression:

$$Q_k = \frac{\sum_{ij} k_{ij}^A \frac{\mu_{ij}^A w_{ij}^A}{\beta_{ij}^A}}{\sum_{ij} k_{ij}^B \frac{\mu_{ij}^A w_{ij}^A}{\beta_{ij}^A}} \tag{11}$$

Here, every variable is taken from simulation A, except for the parameter k_{ij} which comes from simulation A in the numerator and from simulation B in the denominator. In other words, the numerator of the quotient Q_k is simply the rate constant estimate for simulation A. The denominator is identical, except that the parameter k_{ij} has been swapped out for that from a different model, namely from B. This metric Q_k therefore quantifies the influence the gas transfer velocity parameterization with respect to a given plume (here the plume from simulation A). Note that because z_0 is a constant and is equal in both models being compared (z_o=10 m) it cancels in these quotients.

The equivalent metric Q_β quantifies the influence of the carbonate system model on the rate constant of a given plume. Finally, the effect of sea-ice cover alone can be isolated by changing only α_{ice} in the expression for k, yielding Q_{ice}. The results for metrics Q_β, Q_{ice} and Q_k are shown in Figures 9 and 10. We computed them for each of the three plumes from CESM2/MARBL (1999 injections) and ECCO-Darwin (for 1999 and 1992 injections). For purposes of this comparison all parameters fields were regridded onto the CESM2/MARBL grid and the sums were computed over that grid.

2.7.2 Differences due to variations in the plume trajectory.

An orthogonal set of metrics examines not only the choice of gas-exchange parameters but the sensitivity of the exchange rate to the plume trajectory itself. For example, keeping the plume-independent parameters k_{ij} and β_{ij} constant across the expression for Q, but instead using plume weights from either model run, yields:

$$Q_{plume} = \frac{\sum_{ij} \frac{k_{ij}}{\beta_{ij}} \mu_{ij}^A w_{ij}^A}{\sum_{ij} \frac{k_{ij}}{\beta_{ij}} \mu_{ij}^B w_{ij}^B}. \tag{12}$$

Q_{plume} gives the ratio of the rate constants between models A and B, solely due to the difference in which the plume is modelled, pretending the actual gas exchange parameters were the same. For example, if the plume represented by w_{ij}^A is transported into a region of higher wind speeds, as opposed to the plume represented by w_{ij}^B, then $log(Q_{plume})$ would be a greater than 0. The common values for k_{ij} and β_{ij} could be taken either model, or an average could be used. In our case, we opted instead to use experimentally determined values taken from the OceanSODA dataset and regridded to the CESM grid.

https://doi.org/10.5194/egusphere-2025-3713
Preprint. Discussion started: 27 August 2025

Q_{plume} is sensitive both to differences in horizontal spread and vertical distribution of the plume. A slightly different metric Q_{surf} can be defined, which assumes that the vertical distribution is exactly equal in both simulations. Here the μ parameters are simply set to a constant for both numerator and denominator and thus cancel out:

$$Q_{surf} = \frac{\sum_{ij} \frac{k_{ij}}{\beta_{ij}} w_{ij}^A}{\sum_{ij} \frac{k_{ij}}{\beta_{ij}} w_{ij}^B} \tag{13}$$

Conversely, the metric Q_{depth} isolates the effect of downwelling by assuming that the horizontal spread is uniform in latitude and longitude, by using the following weighting:

$$Q_{depth} = \frac{\sum_{ij} \frac{k_{ij}}{\beta_{ij}} \mu_{ij}^A}{\sum_{ij} \frac{k_{ij}}{\beta_{ij}} \mu_{ij}^B} \tag{14}$$

This metric focuses of differences in the rate constant due solely to how much alkalinity remains in the surface.

2.7.3 Distinguishing effects of wind speed vs. effects of carbonate system parameterization

If the simulated plume takes a different trajectory, it will encounter different surface-ocean conditions which can alter the equilibration speed, as captured by Q_{surf}. These differences arise either from different wind or different carbonate system conditions. To disambiguate between the two, the following two metrics can be useful:

$$Q_{surf,k} = \frac{\sum_{ij} k_{ij} w_{ij}^A}{\sum_{ij} k_{ij} w_{ij}^B}, \tag{15}$$

which is computed just like Q_{surf} but the β parameter used is simply the spatial average over all β_{ij}. Because it becomes a constant, independent of i and j, it can be taken outside of the sum and consequently cancels out. Likewise

$$Q_{surf,\beta} = \frac{\sum_{ij} \frac{1}{\beta_{ij}} w_{ij}^A}{\sum_{ij} \frac{1}{\beta_{ij}} w_{ij}^B} \tag{16}$$

is computed by using the spatial average over the k_{ij} values, effectively eliminating it from the fraction. By smearing out the value of either variable, any difference in the rate constants can now be attributed solely to the other. As above, values for k_{ij} and β_{ij} are taken from the OceanSODA (Gregor and Gruber, 2021) dataset. The results for metrics Q_{depth}, Q_{surf}, $Q_{surf,k}$ and $Q_{surf,\beta}$ are shown in Figures 11 and 12.

https://doi.org/10.5194/egusphere-2025-3713
Preprint. Discussion started: 27 August 2025

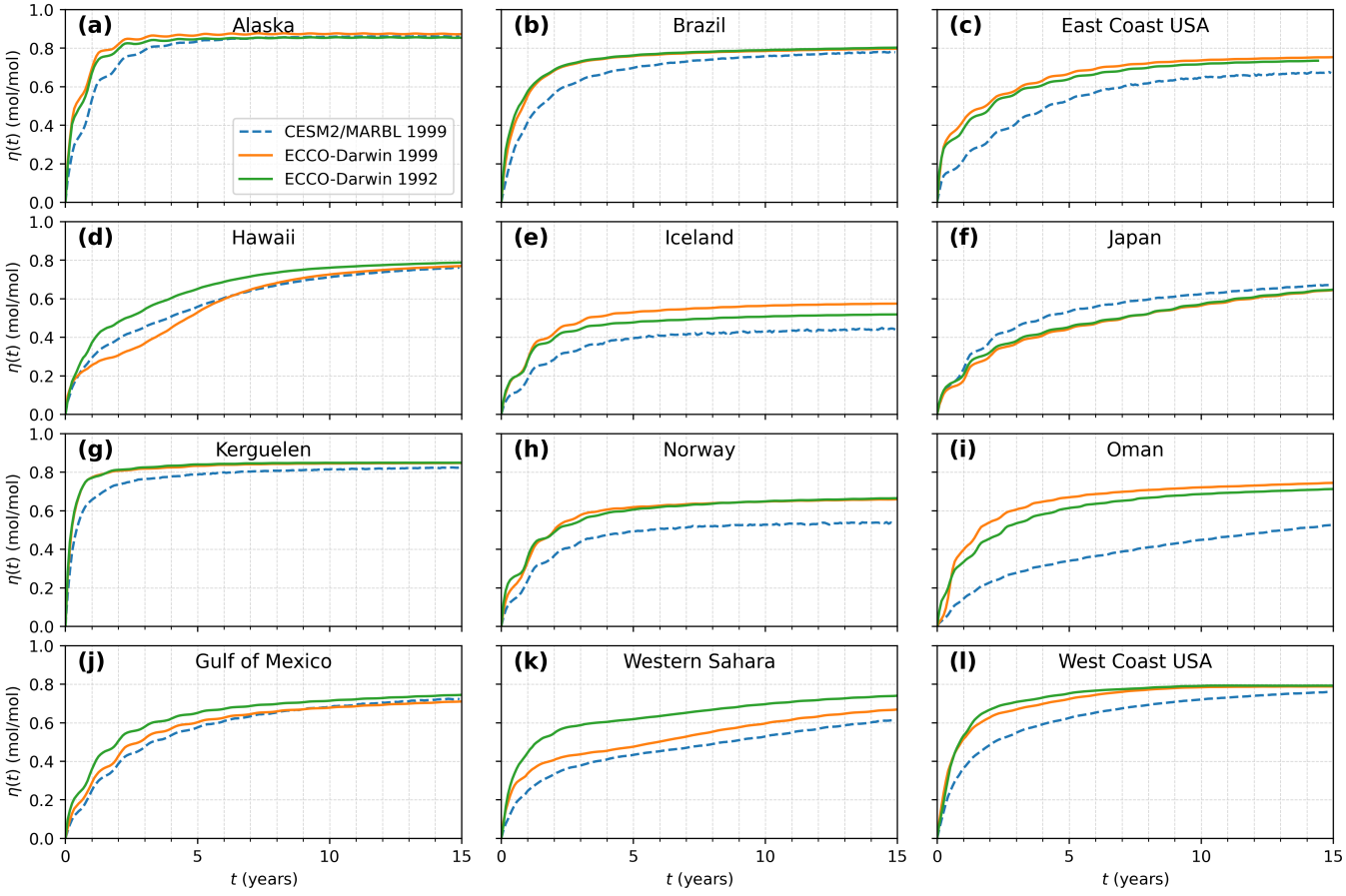

Figure 1. Comparison of OAE uptake efficiency for CESM2/MARBL and ECCO-Darwin model for 12 selected locations.

3 Results

3.1 Comparison of $\eta(t)$ curves

Figure 1 shows a comparison of the OAE equilibration curves ($\eta(t)$) for 12 different locations, obtained from one-month pulse additions of alkalinity in January. For the ECCO-Darwin model, two runs were conducted at each location in 1992 and 1999 to obtain a measure of interannual variability. In many locations, substantial differences between the models are observed, typically larger in magnitude than the interannual difference between the two ECCO-Darwin model runs. In general, the ECCO-Darwin model appears to predict faster equilibration than CESM2/MARBL, the only exception being the alkalinity release in the Kuroshio Current. The largest differences are observed on the west coast of the Sahara, off the coast of Oman as well as releases in the North Atlantic Ocean. The most extreme difference is observed at the Oman location in the Indian Ocean, where the two models disagree up to 50% over the majority of the simulation time, with the discrepancy reducing to

https://doi.org/10.5194/egusphere-2025-3713
Preprint. Discussion started: 27 August 2025

25% by 15 years. Locations near deep-water formation areas, such as offshore of Iceland and Norway, also give substantially different results, with CESM2/MARBL having 25% lower uptake compared to ECCO-Darwin.

In all locations, uptake differences are most pronounced in the first 7 years after release, where $\eta(t)$ can vary up to 50% in extreme cases (such as Oman) but generally differs by $\approx$ 10–20%. After 7 years, the equilibration curves begin to converge again, as the equilibration proceeds towards the theoretically maximal value of ≈ 0.85, the value of which is determined solely by the carbonate chemistry equilibria (Renforth, 2012). This suggests that the models have relatively good agreement in terms of carbonate chemistry, which is expected. However, this convergence is not observed in the North Atlantic Ocean, where the equilibration differences developed by year 7 do not begin to dissipate. In deep-water formation areas, any differences in the initial rate of equilibration have an outsized effect on the progress of the overall equilibration state because equilibration ceases to make progress once the excess alkalinity has been subducted to depth and is isolated from the mixed layer and atmosphere. In other areas of the ocean however, alkalinity is not subducted deep enough and can be transported back to surface-ocean waters on a 5–20 year timescale (Zhou et al., 2024), accounting for the continued equilibration and convergence of the equilibration curves, despite the initial divergence.

3.2 Comparison of the interannual variability

As found by a previous study (Yankovsky et al., 2025), interannual variability within a model is generally non-negligible, making comparison between single runs of different models less statistically meaningful. In order to gain a little insight into the significance of the inter-model differences, we repeated the ECCO-Darwin runs for two different years (1992 and 1999), see Fig. 1. We found that some locations, such as the Amazon and Kerguelen, exhibited virtually no variability, while subtropical locations such as Hawai'i and the west-Saharan coast have substantial differences. Consistent with prior work (Yankovsky et al., 2025), interannual variability itself varies between locations. In general, the interannual differences were significantly smaller than the inter-model differences. A notable exception was the alkalinity release south of Hawai'i, where the two runs diverged considerably; here the CESM2/MARBL run predicts an CO_2 uptake curve intermediate between the two ECCO-Darwin runs.

To further investigate the interannual variability and compare to the previous study of Yankovsky et al. (2025) we repeated the same runs in four of the same locations and in the same years (2000, 2003, 2006, 2009 and 2012) as in their study, with all injections occurring in January. The alkalinity injections occurred in the same geographical areas (as far as the different grids allowed). The results are shown in Figure 2.

First, we note that the amount of interannual variability in ECCO-Darwin and in CESM2/MARBL are correlated, with the largest amount observed in the Gulf Stream location, although it is larger in magnitude in ECCO-Darwin than in CESM2/MARBL for all four cases. Secondly, it is evident that the model differences are considerably larger than interannual variability in all four cases, validating the results from Figure 1. For all four locations, we found that ECCO-Darwin model resulted in substantially faster equilibration during the first 5 years compared to CESM2/MARBL, consistent with our results in the other 12 locations presented earlier. Similar to the earlier experiments, there also appears to be a convergence towards $\eta(t) \approx 0.85$ between equilibration curves from alkalinity injections of different years, in both models. An interesting case is the injection north of Hawai'i,

https://doi.org/10.5194/egusphere-2025-3713
Preprint. Discussion started: 27 August 2025

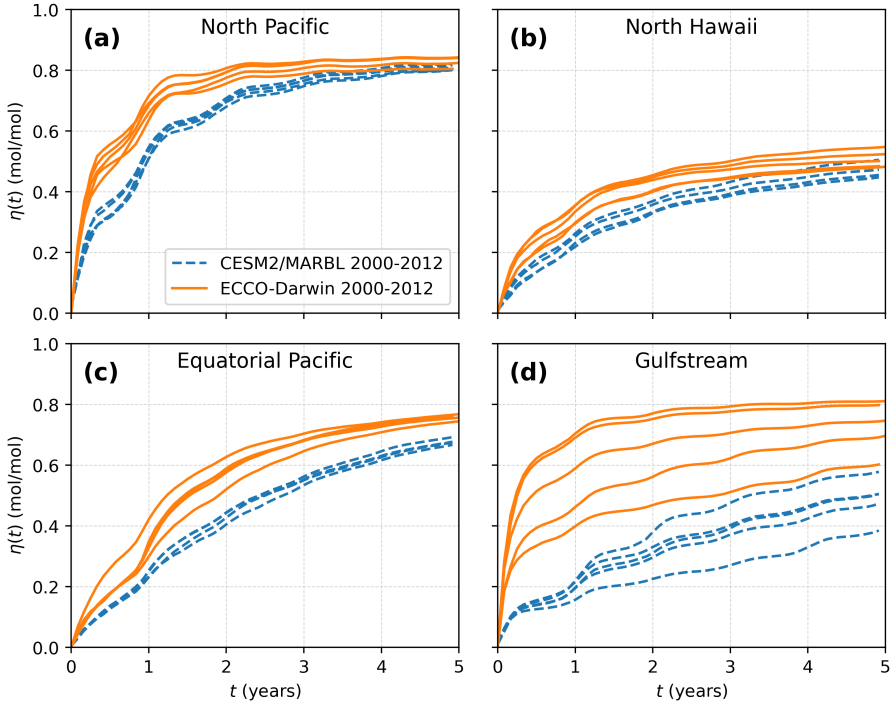

Figure 2. Five year runs with pulse injections in January of 2000, 2003, 2006, 2009 and 2012, compared with results from Yankovsky et al. (2025) for the same locations and years.

which exhibited relatively small interannual variability in ECCO-Darwin as well as CESM2/MARBL. This is in stark contrast to the injection south of Hawai'i (Fig. 1d). It is unclear whether the latter is an outlier or whether the interannual variability is much greater south of Hawai'i.

3.3 Subduction

The equilibration process is dependent on a balance between the rate of CO_2 exchange at the surface ocean and that of subduction processes transporting DIC-deficient water parcels from the surface to depth.

Because the excess alkalinity can only contribute to enhanced CO_2 uptake in the surface-ocean layer of the model, the fraction of the excess alkalinity retained in the surface ocean is an excellent proxy for monitoring the subduction process of the plume (Zhou et al., 2024). The surface-ocean grid cell in both models is 10-m thick, allowing for direct comparison. Figure 3 shows the surface-ocean fraction of excess alkalinity over time for all 12 locations tested.

We find that in locations where there is generally better agreement between the models in terms of CO_2 uptake (Fig. 1), the agreement in terms of surface-ocean alkalinity (Fig. 3) is also better. Conversely, locations with vastly different subduction behavior such as Oman, Norway and west Sahara also have markedly different OAE uptake behavior, with lower modelled

https://doi.org/10.5194/egusphere-2025-3713
Preprint. Discussion started: 27 August 2025

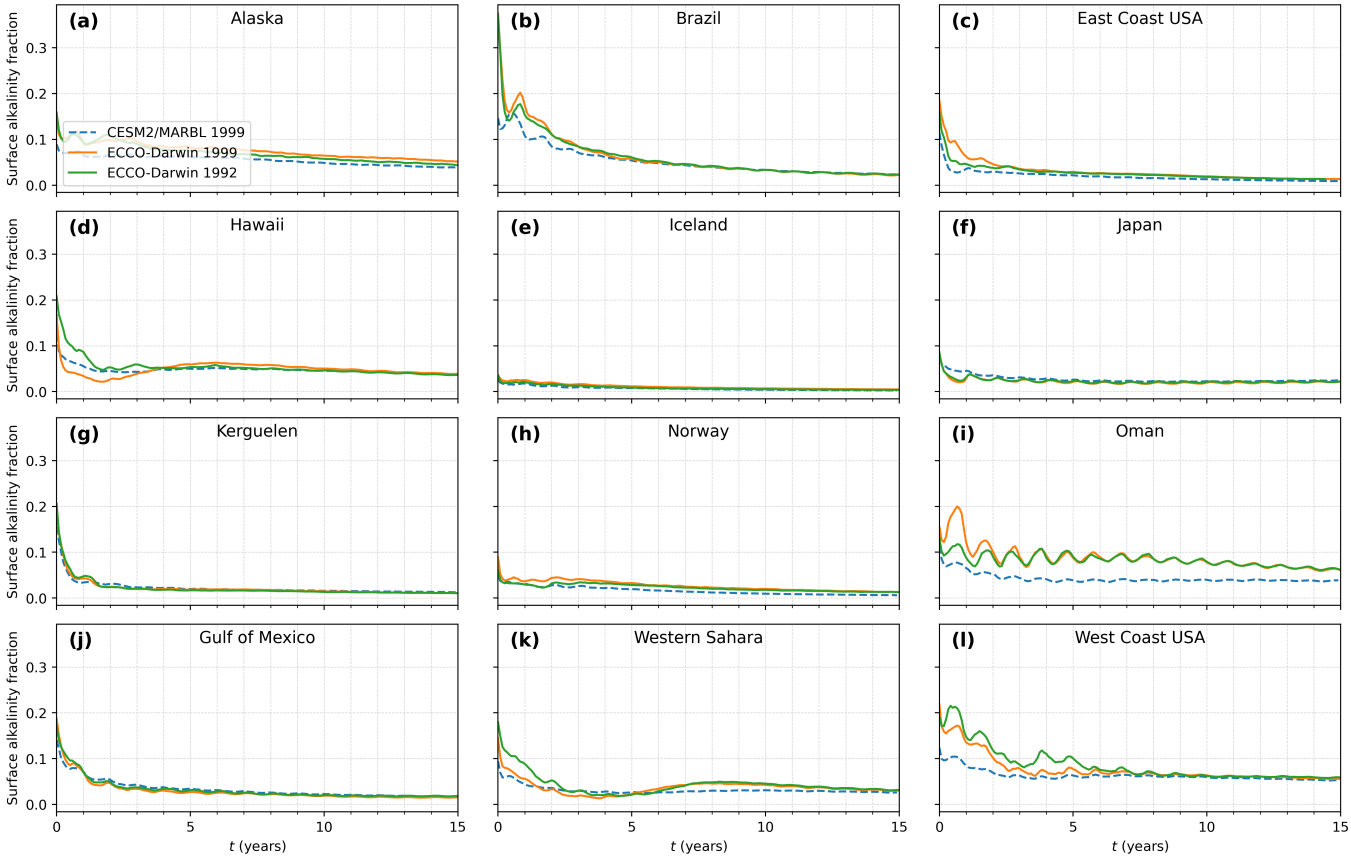

Figure 3. Comparison of the surface fraction of excess alkalinity for CESM2/MARBL and ECCO-Darwin for the 12 tested locations.

surface-ocean alkalinity resulting in much slower CO_2 equilibration. This striking correlation suggests that vertical transport is likely the largest contributor to inter-model differences.

The most pronounced of these differences in our dataset is found at the Oman location. Here, CESM2/MARBL predicts rapid subduction with equilibration slowing significantly after the first two years but continuing at a slow pace, due to gradual remixing of the subducted excess alkalinity. In ECCO-Darwin however, a very different kinetics is observed. Here, subduction occurs much more gradually and the equilibration curve does not exhibit a double exponential shape with two characteristic time constants, as was found by Zhou et al. (2024). In the west Sahara location, both models exhibit the steep subduction followed by rebound, but unlike in the Oman coast; in ECCO-Darwin the rebound is considerably more dramatic and on a different timescale. Overall equilibration can proceed further at an earlier stage and surface-ocean alkalinity stays higher in ECCO-Darwin than in CESM2/MARBL, except in years 2–5. At the Norway coast release location, both models predict excess alkalinity being lost to depth, due to the nearby deep-water formation region. However, the effect is much stronger in CESM2/MARBL, where $\eta(t)$ reaches 0.52 at most, compared with ECCO-Darwin, where it reaches 0.64 (Fig. 1h).

https://doi.org/10.5194/egusphere-2025-3713
Preprint. Discussion started: 27 August 2025

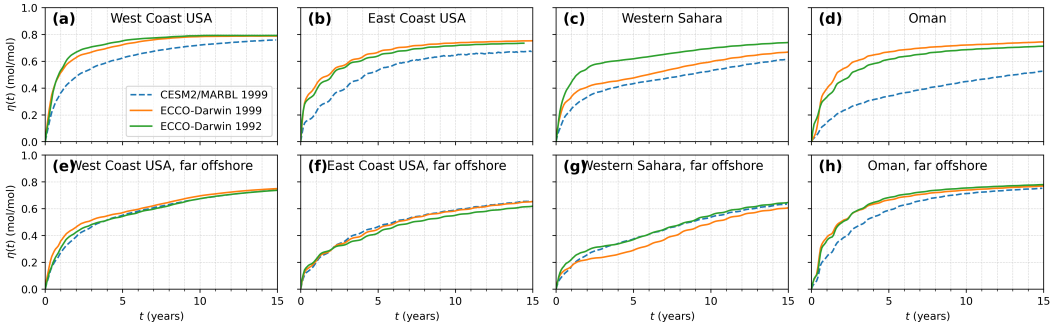

Figure 4. Comparison of OAE equilibration curves from near-coast vs. offshore alkalinity additions.

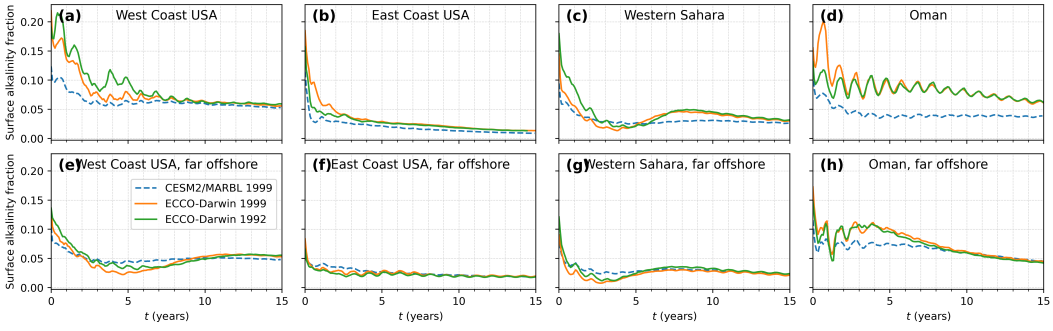

Figure 5. Comparison of surface-ocean excess alkalinity fraction for the same locations as in Fig. 4.

3.4 Coastal locations

To investigate the effect of near-coast ocean dynamics, which could differ substantially between the two models due to their different horizontal grid resolutions and representation of lateral fluxes, we chose four of the earlier locations and repeated the comparisons in a nearby polygon further out in the ocean. The results are shown in Figure 4. We found that in all four cases, the agreement between the two models is considerably greater for offshore locations than for near-shore locations. Furthermore, the interannual variation between the ECCO-Darwin runs conducted in year 1999 and 1992 is also reduced in offshore locations compared to their respective near-shore locations. For all four location, the final values of $\eta(t)$ at 15 years agreed within ± 0.025, but varied as much as ± 0.1 for the equivalent near-shore location. These results are consistent with the idea that the coastal 3-D ocean dynamics are complex and difficult to capture correctly in coarse-resolution ocean models, and may differ more between models compared to simulation of open-ocean waters. In particular, one may expect that lower-resolution models might perform more poorly in the near-coast regimes, and that only higher-resolution models can hope to resolve the complex coastal dynamics. Since near-coast dynamics could lead to substantial upwelling or downwelling currents and intense mixing, such differences would be particularly important for OAE equilibration, since only surface-ocean alkalinity can contribute to CO_2 uptake.

https://doi.org/10.5194/egusphere-2025-3713
Preprint. Discussion started: 27 August 2025

We strengthen this hypothesis by comparing the surface-ocean alkalinity fraction for the same four location pairs (Fig 5). In all four cases, the difference in total excess surface-ocean alkalinity proceeds much more similarly in both models compared to each respective near-coast location. This confirms that near-coast subduction modelling is of primary importance in order to predict the equilibration of near-coast releases. Given that near-coast release of alkalinity is likely to be more economically favorable, this points to a need for greater model certainty in such complex flow regimes. However, the two models we have compared differ in both resolution and parameterization such that we cannot disambiguate which aspect is responsible for the observed differences. Xie et al. (2025) recently reported comparisons between different resolution versions of the same model and found relatively small differences between simulations at 1° and 0.1° resolution; however, locations closer and further from the coast were not explicitly compared.

3.5 Carbonate chemistry

The carbonate chemistry model, in particular at the surface ocean, plays an integral role in the modelling of OAE equilibration. We therefore compare several key quantities between different models, as well as from the data-based OceanSODA product (Gregor and Gruber, 2021) in Figure 6.

Starting with the basic carbonate system tracers $[DIC]$ and $[Alk]$, we find significant differences between the models across latitudes. Compared to OceanSODA, CESM2/MARBL has consistently higher values for both parameters across nearly all latitudes (Fig. 6a,b). ECCO-Darwin exhibits more closely aligned values, although slightly lower than OceanSODA in the near-equatorial latitudes. In the Arctic Ocean however, ECCO-Darwin begins to deviate from the experimental data, while CESM2/MARBL agrees much more closely. However, because [DIC] and [Alk] have compensatory effects on pH and pCO_2, the differences in pCO_2 are somewhat smaller, with the models showing better agreement with each other and with OceanSODA, and mean discrepancies on the order of 10–20 ppm. (Fig. 6d). For comparison the sea-surface temperature (Fig. 6c) exhibits considerably closer agreement between the two models.

Two important sensitivities are of particular importance for OAE. In the short term, the fact that CO_2 is in comparatively fast equilibrium with bicarbonate ions, vastly increases the capacity of seawater to absorb CO_2, but also increases the e-folding time for air-sea CO_2 equilibration. The term $\partial[DIC]/\partial[CO_2]$ is a key sensitivity which quantifies this effect (Middelburg et al., 2020; Zeebe and Wolf-Gladrow, 2001). It is therefore an important parameter to compare between model implementations. Figure 6e shows its mean values across the latitudes, with a larger value leading to slower equilibration. Generally there is quite good agreement, with both models slightly overestimating this sensitivity compared to OceanSODA and therefore overestimating the equilibration e-folding times. The deviation is up to 8–10% for CESM2/MARBL and 2–4% for ECCO-Darwin, with commensurate deviations expected for the equilibration rate constant.

In the long term, after extensive mixing, the equilibration curves will approach a value given by the sensitivity of the carbonate system [DIC] to increases in alkalinity, typically written as $\partial[DIC]/\partial[Alk]$, since it determines the amount of DIC deficit created per unit alkalinity added. The long-term effect on radiative cooling effected by OAE, given the typical lifetime of CO_2 in the atmosphere, occurs on timescales of hundreds of years, by which point alkalinity releases from most locations

https://doi.org/10.5194/egusphere-2025-3713
Preprint. Discussion started: 27 August 2025

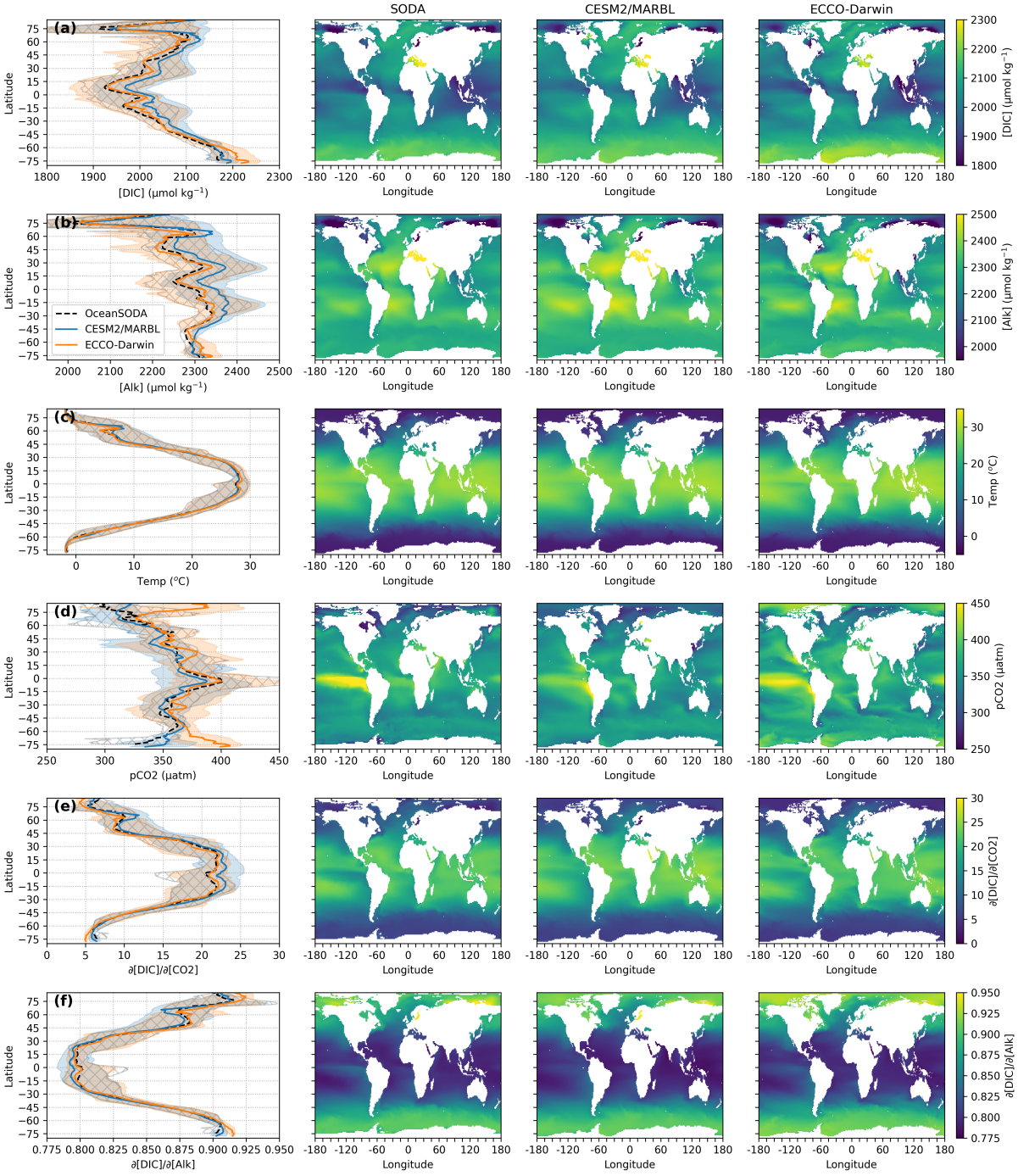

Figure 6. Comparison of surface-ocean carbonate chemistry from CESM2/MARBL model(blue) and ECCO-Darwin (orange), as well as gridded data calculated from OceanSODA (Gregor and Gruber, 2021) (black/hashed) using PyCO2Sys. The pale colored or hashed area denote the 5th and 95th percentiles for each of the three datasets. For the computed meridional averages, the marginal seas were excluded (in particular the Mediterranean, Black, Red, and Baltic seas, the Hudson Bay and the Persian Gulf). Values are time-averaged and plotted against latitude, the spatial axis with the greatest variance. Panels (a) and (b) show $[DIC]$ and total $[Alk]$. Panel (c) shows temperature. Panels (d)–(f) show derived quantities calculated using PyCO2SYS: (d) pCO_2, (e) the carbonate sensitivity $\beta = \partial[DIC]/\partial[CO_2]$ and (f) $\eta_{max} = \partial[DIC]/\partial[Alk]$.

https://doi.org/10.5194/egusphere-2025-3713
Preprint. Discussion started: 27 August 2025

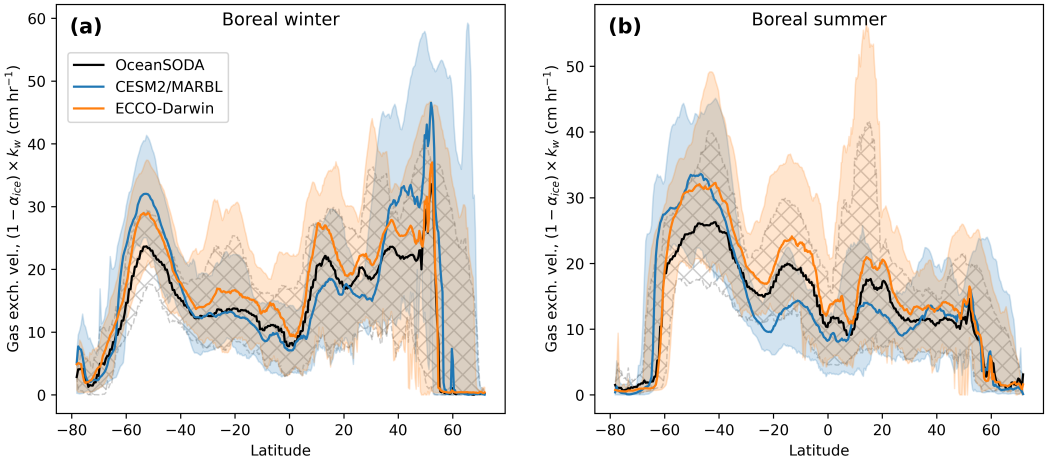

Figure 7. Comparison between the gas exchange velocity k for boreal winter (a) and summer (b) of the year 1999 between CESM2/MARBL, ECCO-Darwin and OceanSODA.

(other than those near deep-water formation areas) will be thoroughly equilibrated. Thus, the end point of the equilibration, i.e., the value of $\partial[DIC]/\partial[Alk]$ is of long-term importance (Zhou et al., 2024; Renforth, 2012) and it is interesting to compare this factor between models. Figure 6f shows that both models agree quite closely, with deviations on the order of a few percent. This suggests that the long-term CO_2 predictions from both models are likely in very good agreement, even if the short-term equilibration e-folding times may differ in each model. This is consistent with a general understanding that the ocean carbonate chemistry is well understood and therefore not a major contributor to the final efficacy of OAE. It is also consistent with our observation that the $\eta(t)$ curves appear to converge in many locations towards the end of the 15-year period simulated here.

3.6 Wind speed

Wind speeds play a central role in determining the speed of gas exchange (Meyer et al., 2018), as the gas transfer velocity k_w is typically parameterized as a function of the square of the wind speed (Wanninkhof, 2014). Figure 7 compares the k parameters calculated for the two models being compared here and OceanSODA. The contribution of sea ice has been included in this comparison. The values for k agree in general, but the details differ substantially. In the boreal summer for example, in the subtropical zones around $\pm 18°$, ECCO-Darwin has k parameters that are nearly 40% higher than those in CESM2/MARBL.

This can be partially explained by the different gas exchange parameterizations in the two models, as noted by Xie et al. (2025). ECCO-Darwin uses the older, but widely adopted parameterization from Wanninkhof (1992) with a higher coefficient of 0.337, while CESM2/MARBL uses a more recent estimate from Wanninkhof (2014) with a coefficient of 0.251, about 25% lower. However, the observed differences in k differ in a more complex way than a simple scaling: the k values in ECCO-Darwin are higher than those from CESM2/MARBL in equatorial regions but lower in polar regions, therefore affecting alkalinity releases at different latitudes in different ways as will be shown later.

https://doi.org/10.5194/egusphere-2025-3713
Preprint. Discussion started: 27 August 2025

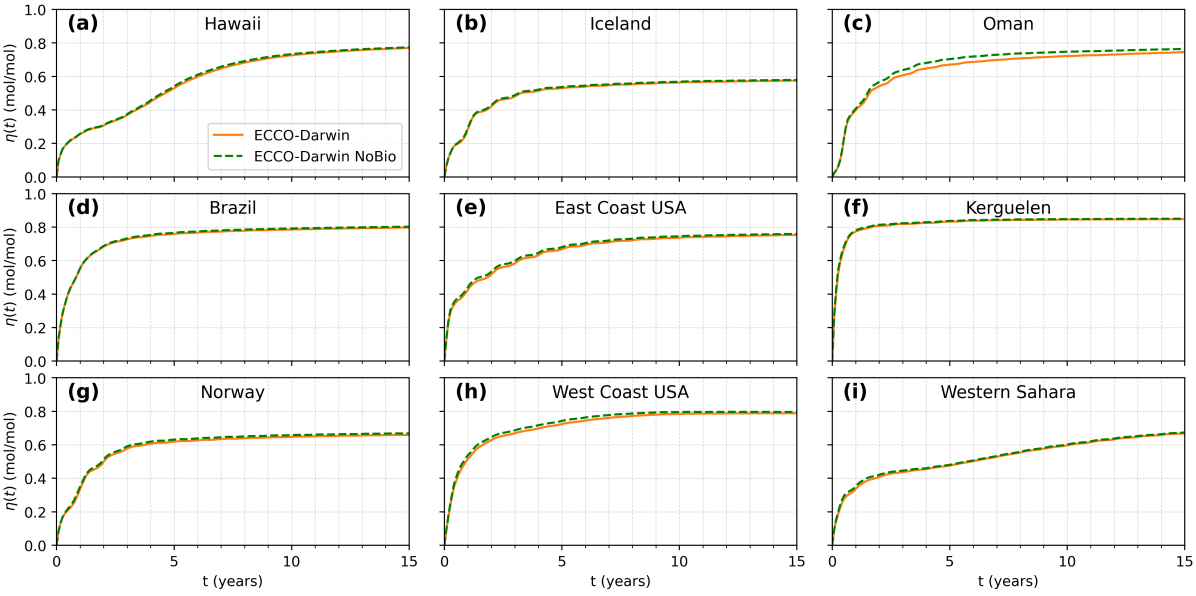

Figure 8. Ablation of biological modelling: The runs labelled "ECCO-Darwin NoBio" have been conducted without biological processes — only the gas-exchange model was enabled.

3.7 Biological processes

As described in the methods, we examined the importance of simulating the soft tissue pump and other biological processes on the equilibration curve by comparing the results of the regular ECCO-Darwin model with an ablated version in which computation of these systems was switched off. The results are shown in Figure 8.

Despite the rather abrupt perturbation to the model, the results show virtually no difference in the equilibration curves with or without biological processes enabled. Despite the sudden removal of biological activity, which causes a steady change in surface DIC and Alk, these changes are virtually equal in the perturbed and the reference simulations and thus for the purpose of calculating the ΔDIC induced by the alkalinity pulse, they appear to cancel. This suggests that OAE impulse response functions can be simulated relatively accurately without reliance on detailed biological models, provided the background carbonate state (vertical DIC and Alk gradients) is accurate to start with. A small difference was observed at the Oman location, however its root cause could not be determined.

Of course, the quantities of alkalinity added in these simulations are quite small and ocean parameters such as pH and carbonate saturation are not dramatically changed. In turn, the rate of biological processes is not impacted significantly. For real-world deployments of OAE this situation may be quite different, and these results here do not apply to the question whether large-scale deployments of OAE could affect biological processes, or cause secondary positive or negative CO_2 uptake feedbacks. However, the shape of the OAE efficiency curves is, in principle, independent of the quantity added (Tyka, 2025), so in that sense the efficiency curves appear to be indeed relatively independent of biological activity. It should be noted that

https://doi.org/10.5194/egusphere-2025-3713
Preprint. Discussion started: 27 August 2025

29 out of 31 tracers were turned off for this experiment, which reduces the computational load substantially. Given the small impact of biology relative to the large impact of circulation, and in particular vertical processes and subduction, it is likely beneficial to focus computational expenditure on higher resolution models rather than sophistication of biological modelling for the purpose of calculating accurate OAE impulse response functions.

3.8 Interaction of plume trajectory and surface exchange parameters

Thus far the analysis has focused on the various aspects of the ocean models which conceivably contribute to CO_2 equilibration dynamics, one at a time: overall surface-ocean dilution and parameterization of gas transfer (i.e., wind speeds, carbonate chemistry parameters and biological processes. However, for any particular release location, the relative importance of these parameters is dependent on the particular trajectory the DIC deficient plume takes, for example, which gas transfer velocities will be encountered by the space-time evolving plume. To disentangle these effects, at least to the extent feasible, we devised a more specific approach which calculates the relative change in the equilibration rate constant based on changing one aspect of the plume at a time as described in detail in the methods section. There are two different approaches this analysis takes. First, we can investigate the effect of changing parameters sets or individual parameters, given a fixed plume trajectory. This investigates the parameterization of the gas exchange, separate from the question of how each model predicts the trajectory of any given plume. As describe in the methods, each parameter can be considered in isolation.

Second, we can investigate the effect of different plume trajectories intersecting a constant set of gas exchange parameters (k and β). This investigates the importance of the predicted flow pattern of each model, separate from the parameterization itself. Again, these effects can further be dissected into contributions from each parameter in turn, by spatially averaging the other parameters to remove their dependence on the plume trajectory.

Figure 13 illustrates an example of alkalinity release near Alaska where three different plume trajectories are overlaid over the gas exchange parameter k. One can clearly see how equilibration will speed up if the plume intersects the high wind speed regions in the North Pacific and avoids the sea-ice covered regions north of the Bering Strait. Likewise, changes in the k parameter would only influence the equilibration if the changes occur along the actual DIC- deficient plume trajectory.

3.8.1 Comparing different parameters sets against a fixed plume trajectory

Figures 9 and 10 show the changes in the equilibration rate-constant with respect to changing the β, sea-ice coverage and k parameterization against a set of fixed plume trajectories. This analysis explicitly excludes differences in the model-dependent circulation flow and focuses on the sensitivity of the equilibration rates with respect to different gas-exchange parameters themselves.

The influence of the carbonate system (specifically β) is relatively modest, $\pm 10\%$ at most, especially once the plumes have spread widely. However, early, when the plume is more localized, the difference can be significant in some locations, with changes on the order of up to $\pm$ 35% in year 1–2. This is consistent with earlier observations that the carbonate system description is very similar in the different models. Probing this difference plume-by-plume however shows that in some cases

https://doi.org/10.5194/egusphere-2025-3713
Preprint. Discussion started: 27 August 2025

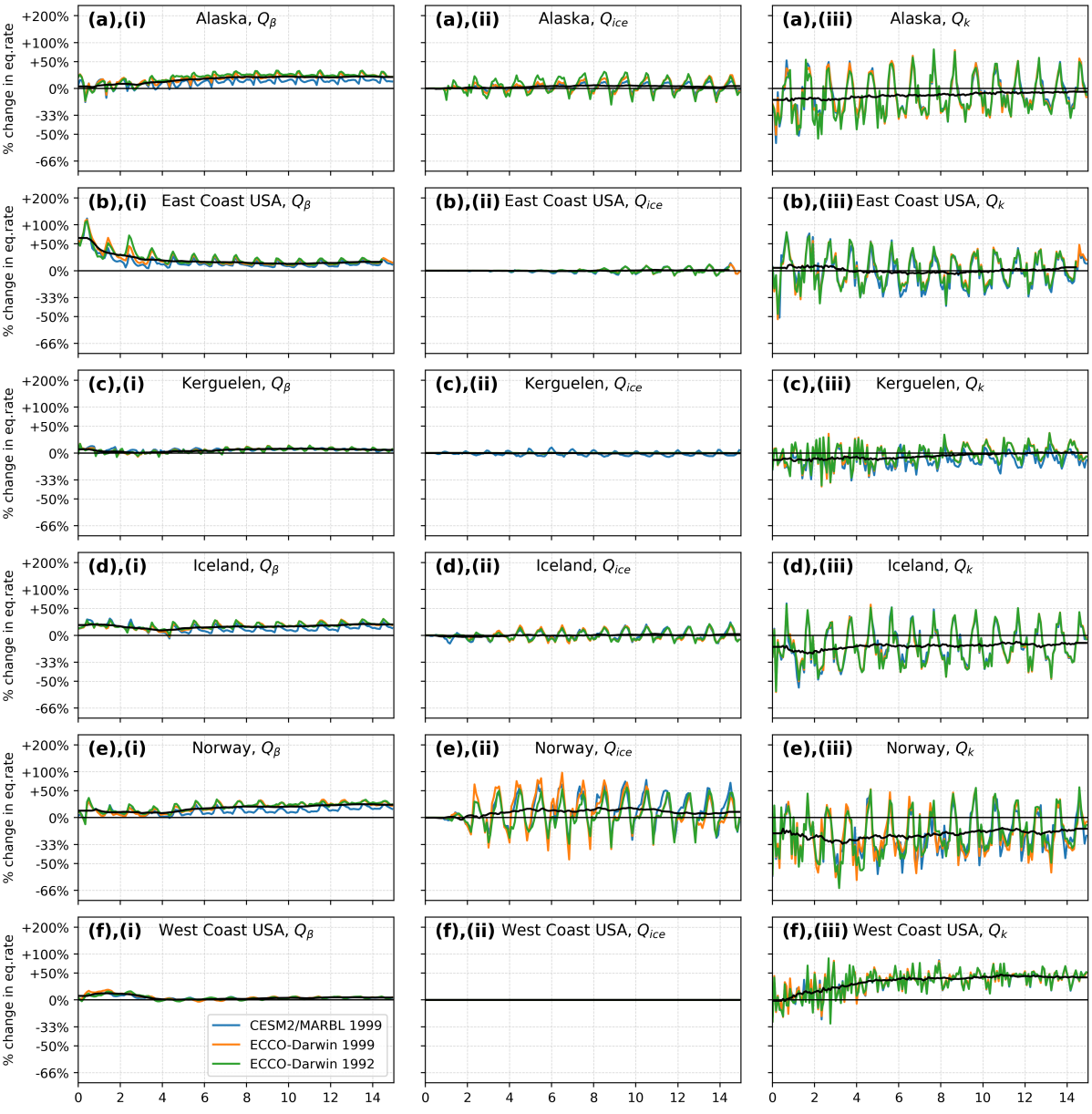

Figure 9. High-latitude locations: relative difference in the equilibration rate constant for a given plume (taken from CESM2/MARBL 1999 (blue), ECCO-Darwin 1999 (orange), or ECCO-Darwin 1992 (green)) for locations **a-f**, if a given gas-exchange parameter (panel columns **i-iii**, β, ice coverage and k (which includes the effect of ice), is changed from the CESM2/MARBL parameter set to the ECCO-Darwin parameter set. Values above 0% indicate equilibration is faster in the ECCO-Darwin gas-exchange parameters set compared to the CESM2/MARBL parameter set.

https://doi.org/10.5194/egusphere-2025-3713
Preprint. Discussion started: 27 August 2025

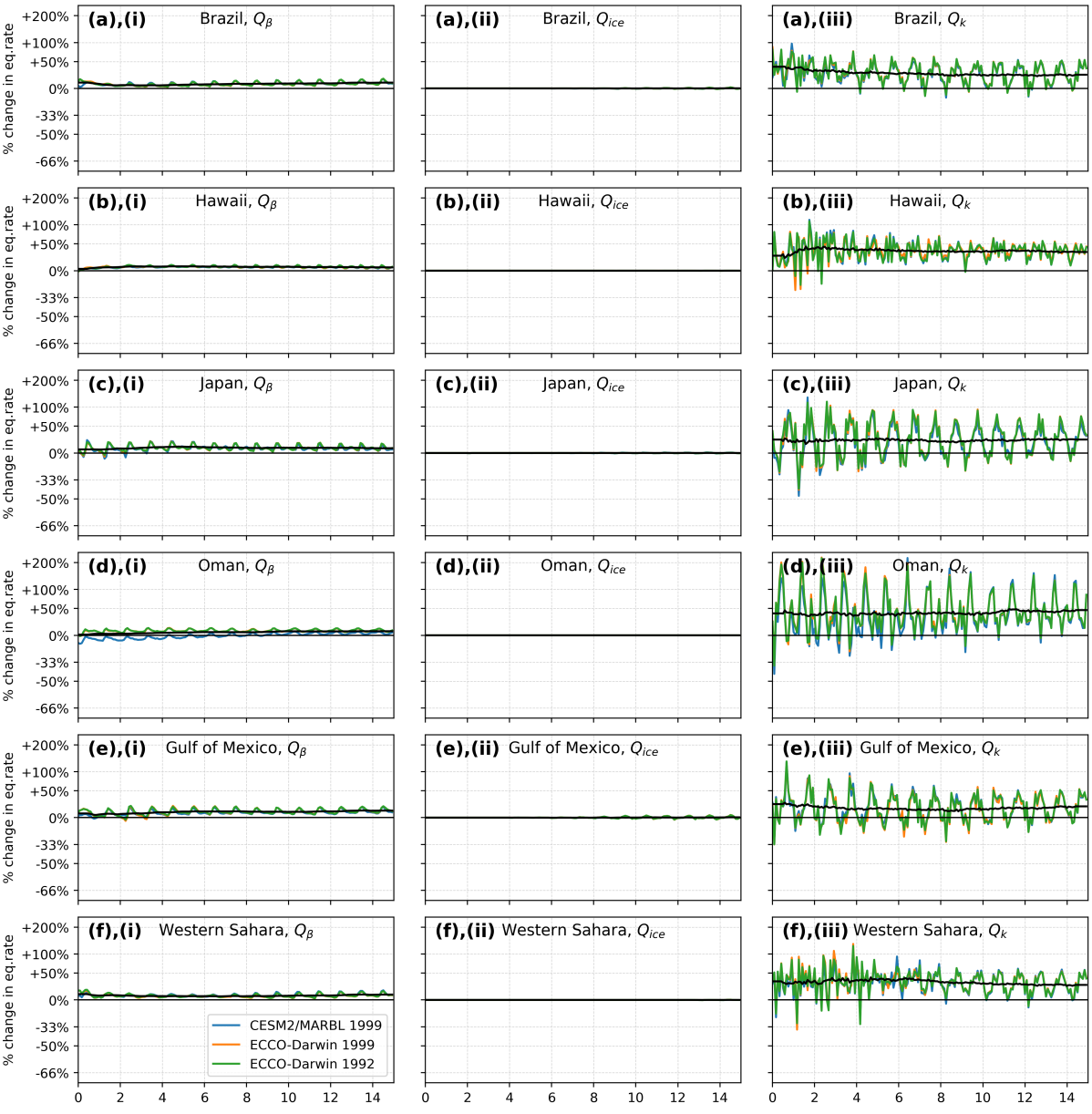

Figure 10. Near-equatorial locations: relative difference in the equilibration rate constant for a given plume (taken from CESM2/MARBL 1999 (blue), ECCO-Darwin 1999 (orange), or ECCO-Darwin 1992 (green)) for locations **a-f**, if a given gas-exchange parameter (panel columns **i-iii**, β, ice coverage and k (which includes the effect of ice), is changed from the CESM2/MARBL parameter set to the ECCO-Darwin parameter set. Values above 0% indicate equilibration is faster in the ECCO-Darwin gas-exchange parameters set compared to the CESM2/MARBL parameter set.

https://doi.org/10.5194/egusphere-2025-3713
Preprint. Discussion started: 27 August 2025

differences in carbonate parameterization can nevertheless affect the resultant CO_2 equilibration behavior. In particular on the east coast of North America the carbonate parameterization of ECCO-Darwin predicts a 60% faster equilibration than in CESM2/MARBL in the first year (Figure 9 a,i). Similar but smaller deviations seen in the northern locations such as Alaska, Iceland and Norway. This discrepancy is much smaller for the more equatorial locations (less than 10%) but in the same direction. These observations are consistent with the earlier comparison of β across latitudes (see Fig. 6 e), where β in ECCO-Darwin is consistently smaller than in CESM2/MARBL, resulting in faster equilibration.

The influence of the sea-ice parameterization is evident for all high-latitude locations (Figure 10, a–f, ii), as any part of the plume which is covered by sea ice is excluded from gas exchange; in particular Norway, followed by Alaska and Iceland, exhibit the highest sensitivities, with strong seasonal variation. However, the difference in ice coverage between models appears to be seasonally compensating, such that the 12-month moving average is generally close to 0%. In the Norway release location however, there appears to be a net bias, where the ECCO-Darwin ice parameterization appears to predict faster equilibration, i.e., lesser sea-ice coverage for the northbound part of the plume. As expected, for more-equatorial release locations, ice coverage has no influence (Figure 10, a–f, ii), except for the Gulf of Mexico, where towards the end of the trajectory the alkalinity reaches the North Atlantic Ocean.

Finally, the wind parameterizations appear to play the largest role in determining equilibration rates (in general, second only to vertical transport, see Figure 11). Interestingly, in high-latitude locations the equilibration appears to be consistently slower in ECCO-Darwin, while for near-equatorial locations it appears to be somewhat faster. This is consistent with the general observation that k_w values from ECCO-Darwin exceed those from CESM2/MARBL in the tropics, but are generally lower than those from CESM2/MARBL towards the poles (see Figure 7), a pattern especially pronounced in the boreal winter. The most extreme difference is found in the Norway release location, followed by the Alaska location, where considerably slower winds are encountered in the ECCO-Darwin 1999 run, compared to CESM2/MARBL. The high sensitivity to sea-ice and wind parameters means that such northern locations are among the more difficult to predict correctly. However, using satellite observational data, sea-ice coverage is relatively easy to monitor and wind speed information is moderately easy to obtain from reanalysis products, such that in a real MRV scenario these parameters could be constrained from observation in near real time, in a post-diction simulation.

3.8.2 Comparing different plume trajectories against fixed parameter sets

Figures 11 and 12 show the change in the rate constant in the ECCO-Darwin runs (1999 and 1992), relative to CESM2/MARBL, when the alkalinity plume from either model run is applied to a constant set of k and carbonate parameters. The latter were taken from the OceanSODA dataset. Values above 0% indicate faster equilibration in ECCO-Darwin compared to CESM2/MARBL. These results probe specifically the sensitivity of CO_2 equilibration on the trajectory of the alkalinity plume, rather than the parameters themselves.

The first column examines the effects of the resident surface alkalinity, Q_{depth}, similar to Figure 3. We find that the effects of vertical transport have by far the largest effect on the equilibration rate constant, especially during the first 4–5 years of the equilibration process. ECCO-Darwin generally yields a higher proportion of alkalinity remaining in the surface layer and

https://doi.org/10.5194/egusphere-2025-3713
Preprint. Discussion started: 27 August 2025

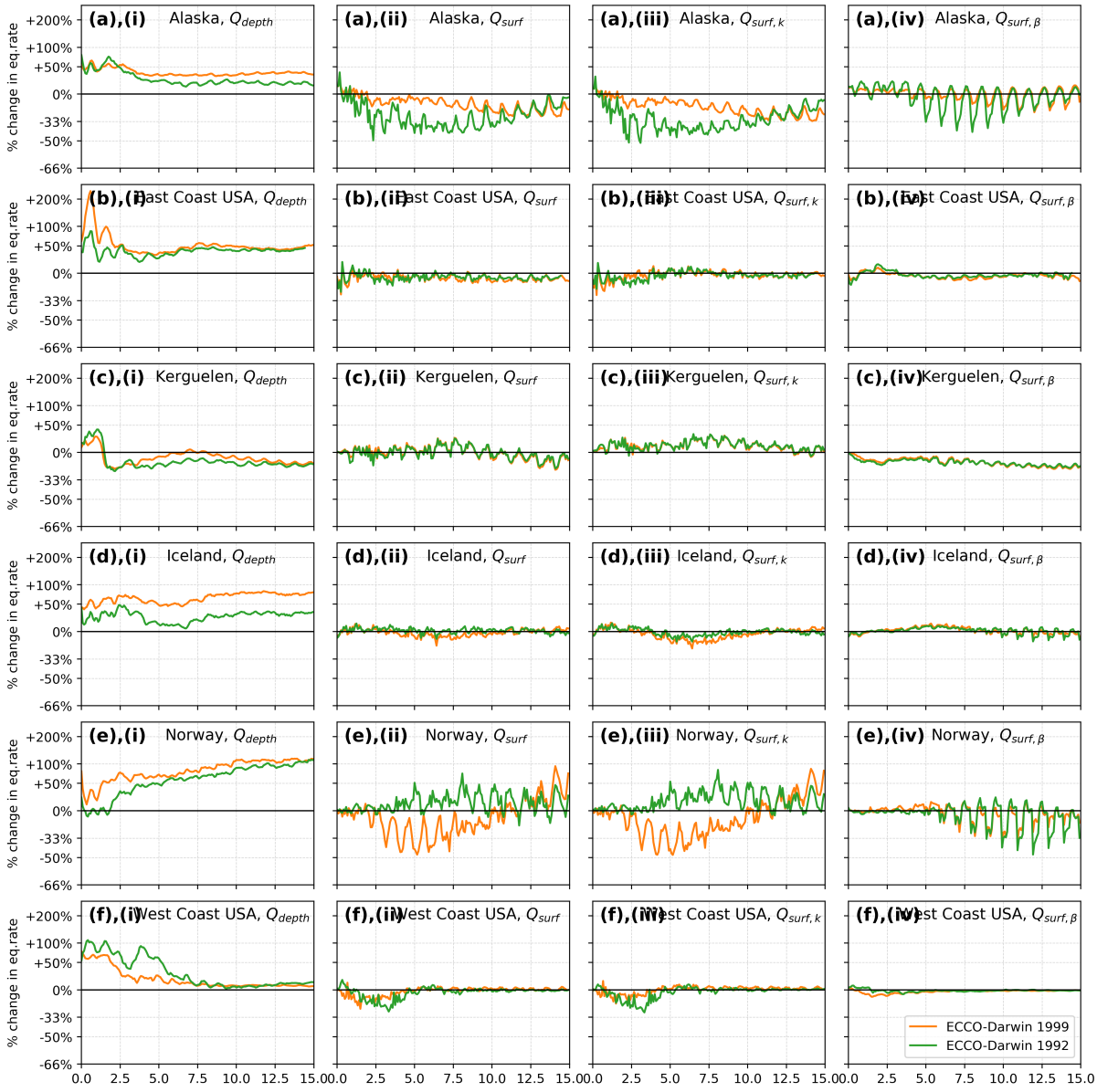

Figure 11. High-latitude release locations: Changes in equilibration rate constant caused by differences in plume dispersion. Gas exchange parameters were set to values from OceanSODA while alkalinity plumes were taken from the CESM2 and ECCO runs, respectively. Plotted values give the relative difference caused by the ECCO plume trajectory relative to the CESM2 trajectory (values larger than 0% mean that the ECCO-Darwin plume causes faster equilibration). a) Only vertical dispersion. b) Only horizontal plume dispersion. c) Horizontal plume dispersion, only with respect to wind and sea-ice cover. d) Horizontal plume dispersion, only with respect to carbonate buffer.

https://doi.org/10.5194/egusphere-2025-3713
Preprint. Discussion started: 27 August 2025

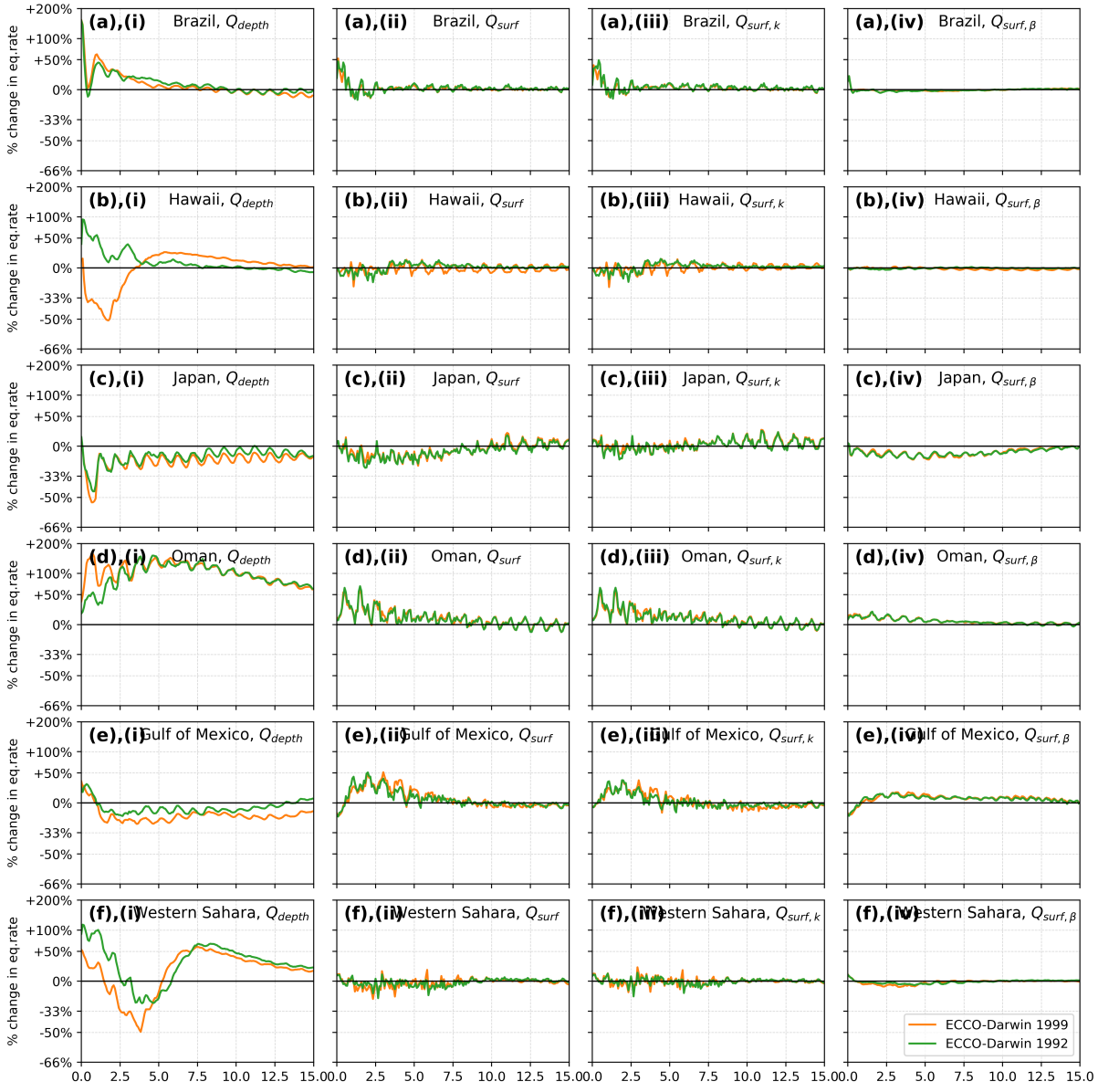

Figure 12. Near-equatorial release locations: Changes in equilibration rate constant caused by differences in plume dispersion. Gas exchange parameters were set to values from OceanSODA while alkalinity plumes were taken from the CESM2 and ECCO runs, respectively. Plotted values give the relative difference caused by the ECCO plume trajectory relative to the CESM2 trajectory (values larger than 0% mean that the ECCO-Darwin plume causes faster equilibration). a) Only vertical dispersion. b) Only horizontal plume dispersion. c) Horizontal plume dispersion, only with respect to wind and sea-ice cover. d) Horizontal plume dispersion, only with respect to carbonate buffer.

https://doi.org/10.5194/egusphere-2025-3713
Preprint. Discussion started: 27 August 2025

therefore faster equilibration. In several places, such as Norway, Gulf Stream, Oman and West Sahara, however, the difference in vertical distribution persists up to 15 years post release and beyond. Sustained equilibration rate differences up to 100% are observed in some places and likely explain the bulk of the differences in the observed $\eta(t)$ curves of Figure 1.

In some cases, such as Hawai'i, there appear to be a large interannual difference in surface alkalinity from 1992 to 1999, with the resulting $\eta(t)$ taking on complex shapes (Fig 3d). For most of the remaining locations, however, there appears to be relatively good agreement between the two ECCO-Darwin years examined, with moderate differences observed in Iceland, Norway, Alaska and Western Sahara.

The second columns of Figure 11 and 12 consider only the horizontal distribution of the plume, while keeping the surface alkalinity fraction equal, i.e. Q_{surf}. For the more equatorial locations (Fig. 12) only relatively small differences remain ($\pm$15%), once the vertical alkalinity distributions are factored out, which quickly decay towards zero. In the set of high-latitude locations (Fig. 11) however, we observe several locations which exhibit a very significant influence of horizontal plume dispersal on the equilibration rate that the plume encounters, in particular Norway and Alaska, with the effect increasing in time as the difference in the plumes increases.

In both these cases, there is also significant interannual variation in the horizontal dispersion case (columns 2–4), which was not as evident when looking at the vertical dispersion case (column 1). In the case of the Norway release location, the ECCO-Darwin 1999 trajectory appears to lead to a reduction of equilibration rate relative to CESM2/MARBL by up to 50% at its extreme, while the 1992 trajectory lead to an increase in the equilibration rate of up to 50%.

What causes such large sensitivities on plume trajectories? In extreme northern (and to a lesser degree extreme southern) latitudes, the equilibration parameters k and β go through very significant changes with latitude (see Figures 6 and 7). In addition, the sea-ice cover boundary is very near. Therefore, the precise trajectory a plume takes can have a very significant effect on equilibration kinetics for release locations near such transition zones. On the contrary, releases for which the plume generally remains equatorial, where the equilibration parameters are more uniform, do not exhibit such sensitivities.

Figure 13 shows an example of such a situation. Three different plume extents are displayed over a background shading of the k parameter. One can see intuitively how, depending on the extent to which the plume traverses the Bering straight into sea-ice covered regions, or its southwards trajectory into or out of high-wind regions of the central North Pacific, the overall equilibration rate constant can vary dramatically.

The effects of the horizontal distribution can also be analyzed separately with respect to the plume encountering different wind/sea ice (column 3, $Q_{surf,k}$) and carbonate conditions (column 4, $Q_{surf,\beta}$). In the near-equatorial locations, differences in plume-encountered wind shear appear to make the majority of the contributions, with carbonate chemistry differences only evident in the Japan and Oman release locations. The carbonate system parameter β is almost constant between the latitudes -30° S and 30° N (Fig. 6. Unsurprisingly, for releases that are closer to the equator (Amazon, Hawai'i, Western Sahara, Gulf of Mexico, Oman), changes in plume dispersion don't change the effective β very much and correspondingly, $Q_{surf,\beta}$ is close to 1.0. In high-latitude locations, the contributions are more equally shared (as both parameters go through significant latitudinal changes), with slightly more sensitivity attributable to wind. For all parameters, seasonal variations are evident.

https://doi.org/10.5194/egusphere-2025-3713
Preprint. Discussion started: 27 August 2025

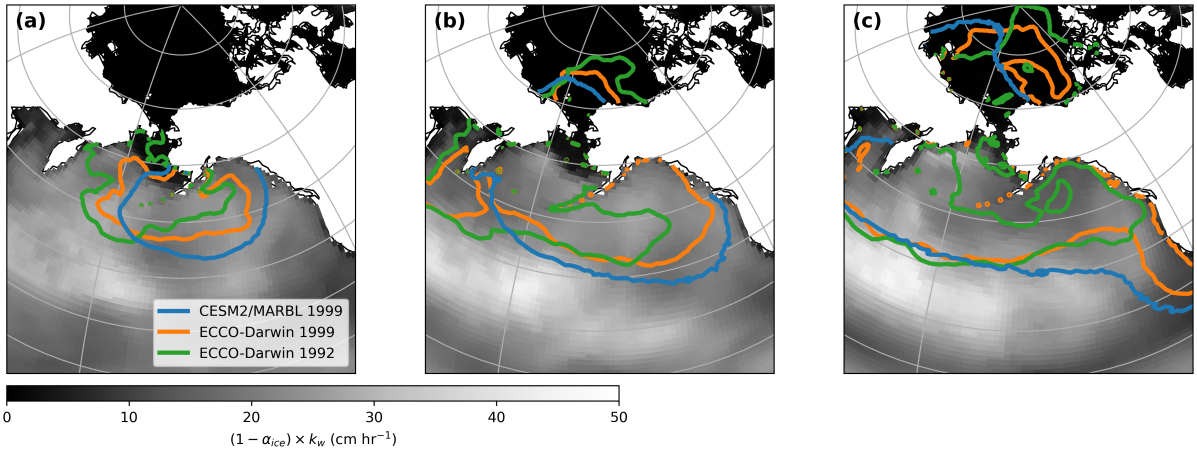

Figure 13. Three different plume outlines overlaid on the k parameter in greyscale from OceanSODA(Gregor and Gruber, 2021) after a) 12 b) 36 and c) 72 month after alkalinity release near Alaska.

Overall, the difference in plume trajectory that appears to have the greatest effect on the overall equilibration is the vertical alkalinity distribution (Q_{depth}). This sensitivity to vertical transport is not surprising because excess alkalinity can only drive ocean CO_2 uptake while it is resident in the surface-ocean layer. Additionally however, it is likely that the data-driven parameterization of vertical transport is the least well constrained and thus the model-differences in vertical transport may also be larger than horizontal differences.

https://doi.org/10.5194/egusphere-2025-3713
Preprint. Discussion started: 27 August 2025

4 Limitations and Conclusions

Due to the complexity of the variables at play, the sheer number of different ocean models that have been developed and the lack of direct measurements of CO_2 equilibration at basin scale, this work cannot possibly give a comprehensive conclusion to the question of how accurate ocean models are at predicting OAE-based CO_2 uptake. This paper is therefore intended as a first preliminary exploration of the possible effects of different model parameterizations and hopes to serve as a starting point for further research; many aspects and interesting questions have not yet been explored due to limitations in available computing and analysis resources. All alkalinity releases were conducted in January, so further work remains to quantify how these discovered differences translate to other release months at various global locations. This is important, since previous work has revealed considerable seasonal differences in uptake curves (Zhou et al., 2024; Suselj et al., 2025), plume trajectories, and background air-sea equilibration timescales (Jones et al., 2014). Interannual variance was also only addressed minimally for most locations, with only a small amount of insight gained for a selected few locations. The most significant limitation is of course the fact that we were only able to compare two models; a large-scale OAE inter-model comparison is sorely needed to gain more insights into the model variance.

While the two models used here have somewhat different resolution (1° vs 1/3°) we are unable to disambiguate whether the differences in plume trajectories arise from differences in forcing parameterization or the resolution itself. However, resolution differences within the same model framework were recently studied by Xie et al. (2025) and relatively small differences were found, suggesting that the strong differences observed in the present study arise from differences in the forcing and parameterization, rather than the explicit grid resolution. However, there is the caveat that resolution hierarchies in other models may exhibit more profound differences owing to grid resolution, depending on scale-dependent parameterization choices employed as resolution changes. Further, Xie et al. (2025) only investigated resolution differences down to 0.1°, which may not be fine enough to reveal the effect of complex coastal-ocean flows. Coastal areas are regions of intense submesoscale dynamics, known to create higher vertical velocities, thus more research will be necessary to establish the importance of submesoscale-resolving simulation on OAE efficiency calculations.

We have compared OAE-based CO_2 uptake curves for two different resolution models, the 1.0° CESM2/MARBL based model used by Zhou et al. (2024) and the ECCO-Darwin 1/3° model, based on 12 pulse-release experiments conducted in both models in the month of January at matched locations. The ECCO-Darwin-based experiment was also repeated in year 1992 and 1999. We find that significant and complex differences in the equilibration trajectories are evident in almost all locations. In general the ECCO-Darwin model predicts faster equilibration timescales than CESM2/MARBL. The most significant deviations occur in the near-term (years 1–7) with a degree of convergence towards DIC/Alk$\approx$0.85 observed in many but not all locations. Near-coast locations were found to have greater disagreements than offshore locations.

We further examined the root causes of these differences, including primary differences in the gas-exchange parameterization itself (wind speeds, sea-ice cover, carbonate parameters) and secondary differences in the flow field predicted by the various models. Overall, the largest contributor was found to be the vertical transport and mixing of surface alkalinity, consistent with results from Suselj et al. (2025). The second-largest contributor was the wind parameterization. More minor changes

https://doi.org/10.5194/egusphere-2025-3713
Preprint. Discussion started: 27 August 2025

arise from differences in the carbonate system parameters, which were found to be more aligned between models. Horizontal plume trajectories also were found to play a role, however this varied considerably from location to location, with some of the high-latitude locations being quite sensitive to different plume trajectories, while equatorial locations were not. The role of biological activity was assessed, and its effect on the shape of the equilibration curves was found to be almost negligible.

Given the variations observed, even when only examining two models, much more experimental data will be needed to constrain simulations and narrow the variance observed in OAE uptake predictions. In particular, it appears that vertical transport is not sufficiently constrained, especially in near-coastal areas, where the dynamics and three-dimensional flows may be quite complex. Higher-resolution models or coarser models with unstructured fine-scale grids in the coastal zone (Ward et al., 2020) should in principle give more realistic flow patterns and vertical mixing predictions towards the coast. Thus, it would be useful for future work to examine whether high-resolution models give closer mutual agreement compared to coarser-resolution models, especially across the coastal and nearshore zone (Anderson et al., 2025). It may be, however, that more high-resolution experimental data, especially for deeper parts of the ocean, will be needed to verify and constrain simulations. Besides differences in model resolution and parameterization, we note that the inter-model differences described in this paper may also arise from the use of physical and biogeochemical data assimilation in ECCO-Darwin, which could lead to more-accurate representation of the physical-biogeochemical ocean state. Notably, CESM2/MARBL is known to exhibit several biases in ocean physics, in particular mixed layer depth, which will impact OAE equilibration timescales (Griffies et al., 2009; Danabasoglu et al., 2014).

On the other hand, since the behavior of small water parcels close to the original injection site is inherently chaotic, there may exist inherent limits to the reliability any simulation can achieve even in the limit of realistically modelled physics, when the precise motion and forcings at the time of release can never be measured to a sufficiently fine degree. Here, only direct experimental tracking of the spreading plume can help fill the knowledge gap. Once sufficiently dispersed, effects of local chaos are reduced and a more averaged, and more aggregate behavior could be expected, amenable to ocean models. In that sense, the ultimate MRV approach will likely require a close interplay between experimental near-field measurements and far-field simulations.

Code and data availability. Code and data will be made available upon publication.

Author contributions. MDT and MZ conceived of the study, MDT conducted simulations using ECCO-Darwin and conducted the comparison analysis and prepared figures, MZ and EY conducted simulations using CESM2/MARBL, MDT, MZ, EY and DC wrote the manuscript

https://doi.org/10.5194/egusphere-2025-3713
Preprint. Discussion started: 27 August 2025

Acknowledgements. The authors would like to express their gratitude to Chris Van Arsdale, and Yinghuan Xie for many helpful comments on the paper. DC acknowledges support from the NASA Carbon Monitoring System program. MZ and EY acknowledge the support from Yale Center for Natural Carbon Capture.

https://doi.org/10.5194/egusphere-2025-3713
Preprint. Discussion started: 27 August 2025

References

Anderson, H., Mongin, M., and Matear, R.: Ocean alkalinity enhancement in a coastal channel: simulating localised dispersion, carbon sequestration and ecosystem impact, Environmental Research Communications, 7, 041 012, 2025.

Andrews, A. E., Kofler, J. D., Trudeau, M. E., Williams, J. C., Neff, D. H., Masarie, K. A., Chao, D. Y., Kitzis, D. R., Novelli, P. C., Zhao, C. L., Dlugokencky, E. J., Lang, P. M., Crotwell, M. J., Fischer, M. L., Parker, M. J., Lee, J. T., Baumann, D. D., Desai, A. R., Stanier, C. O., De Wekker, S. F. J., Wolfe, D. E., Munger, J. W., and Tans, P. P.: CO_2, CO, and CH_4 measurements from tall towers in the NOAA Earth System Research Laboratory's Global Greenhouse Gas Reference Network: instrumentation, uncertainty analysis, and recommendations for future high-accuracy greenhouse gas monitoring efforts, Atmospheric Measurement Techniques, 7, 647–687, https://doi.org/10.5194/amt-7-647-2014, 2014.

Bach, L. T., Ho, D. T., Boyd, P. W., and Tyka, M. D.: Toward a consensus framework to evaluate air-sea CO2 equilibration for marine CO2 removal, Limnology and Oceanography Letters, 8, 685–691, https://doi.org/https://doi.org/10.1002/lol2.10330, 2023.

Broecker, W. and Peng, T.: Tracers in the Sea, Eldigio Press/Columbia University, New York, ISBN 978-9993186724, 1982.

Carroll, D., Menemenlis, D., Adkins, J. F., Bowman, K. W., Brix, H., Dutkiewicz, S., Fenty, I., Gierach, M. M., Hill, C., Jahn, O., Landschützer, P., Lauderdale, J. M., Liu, J., Manizza, M., Naviaux, J. D., Rödenbeck, C., Schimel, D. S., Van der Stocken, T., and Zhang, H.: The ECCO-Darwin Data-Assimilative Global Ocean Biogeochemistry Model: Estimates of Seasonal to Multidecadal Surface Ocean pCO2 and Air-Sea CO2 Flux, Journal of Advances in Modeling Earth Systems, 12, e2019MS001 888, https://doi.org/https://doi.org/10.1029/2019MS001888, e2019MS001888 2019MS001888, 2020.

Carroll, D., Menemenlis, D., Dutkiewicz, S., Lauderdale, J. M., Adkins, J. F., Bowman, K. W., Brix, H., Fenty, I., Gierach, M. M., Hill, C., Jahn, O., Landschützer, P., Manizza, M., Mazloff, M. R., Miller, C. E., Schimel, D. S., Verdy, A., Whitt, D. B., and Zhang, H.: Attribution of Space-Time Variability in Global-Ocean Dissolved Inorganic Carbon, Global Biogeochemical Cycles, 36, e2021GB007 162, https://doi.org/https://doi.org/10.1029/2021GB007162, e2021GB007162 2021GB007162, 2022.

Carroll, D., Menemenlis, D., Zhang, H., Mazloff, M., McKinley, G., Fay, A., Dutkiewicz, S., Lauderdale, J., and Fenty, I.: Evaluation of the ECCO-Darwin Ocean Biogeochemistry State Estimate vs. In-situ Observations, https://doi.org/10.5281/zenodo.10627664, 2024.

Danabasoglu, G., Yeager, S. G., Bailey, D., Behrens, E., Bentsen, M., Bi, D., Biastoch, A., Böning, C., Bozec, A., Canuto, V. M., Cassou, C., Chassignet, E., Coward, A. C., Danilov, S., Diansky, N., Drange, H., Farneti, R., Fernandez, E., Fogli, P. G., Forget, G., Fujii, Y., Griffies, S. M., Gusev, A., Heimbach, P., Howard, A., Jung, T., Kelley, M., Large, W. G., Leboissetier, A., Lu, J., Madec, G., Marsland, S. J., Masina, S., Navarra, A., Nurser, A. J. G., Pirani, A., Salas y Mélia, D., Samuels, B. L., Scheinert, M., Sidorenko, D., Treguier, A.-M., Tsujino, H., Uotila, P., Valcke, S., Voldoire, A., and Wangi, Q.: North Atlantic simulations in Coordinated Ocean-ice Reference Experiments phase II (CORE-II). Part I: Mean states, Ocean Modeling, 73, 76–107, https://doi.org/10.1016/j.ocemod.2013.10.005, 2014.

Danabasoglu, G., Lamarque, J.-F., Bacmeister, J., Bailey, D. A., DuVivier, A. K., Edwards, J., Emmons, L. K., Fasullo, J., Garcia, R., Gettelman, A., Hannay, C., Holland, M. M., Large, W. G., Lauritzen, P. H., Lawrence, D. M., Lenaerts, J. T. M., Lindsay, K., Lipscomb, W. H., Mills, M. J., Neale, R., Oleson, K. W., Otto-Bliesner, B., Phillips, A. S., Sacks, W., Tilmes, S., van Kampenhout, L., Vertenstein, M., Bertini, A., Dennis, J., Deser, C., Fischer, C., Fox-Kemper, B., Kay, J. E., Kinnison, D., Kushner, P. J., Larson, V. E., Long, M. C., Mickelson, S., Moore, J. K., Nienhouse, E., Polvani, L., Rasch, P. J., and Strand, W. G.: The Community Earth System Model Version 2 (CESM2), Journal of Advances in Modeling Earth Systems, 12, e2019MS001 916, https://doi.org/https://doi.org/10.1029/2019MS001916, e2019MS001916 2019MS001916, 2020.

https://doi.org/10.5194/egusphere-2025-3713
Preprint. Discussion started: 27 August 2025

Dietze, H. and Oschlies, A.: On the correlation between air-sea heat flux and abiotically induced oxygen gas exchange in a circulation model of the North Atlantic, Journal of Geophysical Research: Oceans, 110, https://doi.org/https://doi.org/10.1029/2004JC002453, 2005.

Dutkiewicz, S., Hickman, A. E., Jahn, O., Gregg, W. W., Mouw, C. B., and Follows, M. J.: Capturing optically important constituents and properties in a marine biogeochemical and ecosystem model, Biogeosciences, 12, 4447–4481, 2015.

Eyring, V., Bony, S., Meehl, G. A., Senior, C. A., Stevens, B., Stouffer, R. J., and Taylor, K. E.: Overview of the Coupled Model Intercomparison Project Phase 6 (CMIP6) experimental design and organization, Geoscientific Model Development, 9, 1937–1958, https://doi.org/10.5194/gmd-9-1937-2016, 2016.

Fekete, B. M., Vörösmarty, C. J., and Grabs, W.: High-resolution fields of global runoff combining observed river discharge and simulated water balances, Global Biogeochemical Cycles, 16, 15–1–15–10, https://doi.org/https://doi.org/10.1029/1999GB001254, 2002.

Fennel, K., Long, M. C., Algar, C., Carter, B., Keller, D., Laurent, A., Mattern, J. P., Musgrave, R., Oschlies, A., Ostiguy, J., Palter, J. B., and Whitt, D. B.: Modelling considerations for research on ocean alkalinity enhancement (OAE), State of the Planet, 2-oae2023, 9, https://doi.org/10.5194/sp-2-oae2023-9-2023, 2023.

Forget, G., Campin, J.-M., Heimbach, P., Hill, C. N., Ponte, R. M., and Wunsch, C.: ECCO version 4: an integrated framework for non-linear inverse modeling and global ocean state estimation, Geoscientific Model Development, 8, 3071–3104, https://doi.org/10.5194/gmd-8-3071-2015, 2015.

Gaspar, P., Grégoris, Y., and Lefevre, J.-M.: A simple eddy kinetic energy model for simulations of the oceanic vertical mixing: Tests at station Papa and long-term upper ocean study site, Journal of Geophysical Research: Oceans, 95, 16 179–16 193, 1990.

Gregor, L. and Gruber, N.: OceanSODA-ETHZ: a global gridded data set of the surface ocean carbonate system for seasonal to decadal studies of ocean acidification, Earth System Science Data, 13, 777–808, https://doi.org/10.5194/essd-13-777-2021, 2021.

Griffies, S. M., Biastoch, A., Böning, C., Bryan, F., Danabasoglu, G., Chassignet, E. P., England, M. H., Gerdes, R., Haak, H., Hallberg, R. W., et al.: Coordinated ocean-ice reference experiments (COREs), Ocean modelling, 26, 1–46, 2009.

He, J. and Tyka, M. D.: Limits and CO_2 equilibration of near-coast alkalinity enhancement, Biogeosciences, 20, 27–43, https://doi.org/10.5194/bg-20-27-2023, 2023.

Ho, D. T., Law, C. S., Smith, M. J., Schlosser, P., Harvey, M., and Hill, P.: Measurements of air-sea gas exchange at high wind speeds in the Southern Ocean: Implications for global parameterizations, Geophysical Research Letters, 33, https://doi.org/https://doi.org/10.1029/2006GL026817, 2006.

Humphreys, M. P., Daniels, C. J., Wolf-Gladrow, D. A., Tyrrell, T., and Achterberg, E. P.: On the influence of marine biogeochemical processes over CO2 exchange between the atmosphere and ocean, Marine Chemistry, 199, 1–11, https://doi.org/https://doi.org/10.1016/j.marchem.2017.12.006, 2018.

Humphreys, M. P., Gregor, L., Pierrot, D., van Heuven, S. M. A. C., Lewis, E. R., and Wallace, D. W. R.: PyCO2SYS: marine carbonate system calculations in Python, https://doi.org/10.5281/ZENODO.3744275, 2020.

Jones, D. C., Ito, T., Takano, Y., and Hsu, W.-C.: Spatial and seasonal variability of the air-sea equilibration timescale of carbon dioxide, Global Biogeochemical Cycles, 28, 1163–1178, https://doi.org/https://doi.org/10.1002/2014GB004813, 2014.

Keller, D. P., Lenton, A., Scott, V., Vaughan, N. E., Bauer, N., Ji, D., Jones, C. D., Kravitz, B., Muri, H., and Zickfeld, K.: The Carbon Dioxide Removal Model Intercomparison Project (CDRMIP): rationale and experimental protocol for CMIP6, Geoscientific Model Development, 11, 1133–1160, https://doi.org/10.5194/gmd-11-1133-2018, 2018.

https://doi.org/10.5194/egusphere-2025-3713
Preprint. Discussion started: 27 August 2025

Kobayashi, S., Ota, Y., Harada, Y., Ebita, A., Moriya, M., Onoda, H., Onogi, K., Kamahori, H., Kobayashi, C., Endo, H., Miyoka, K., and Takahashi, K.: The JRA-55 Reanalysis: General Specifications and Basic Characteristics, Journal of the Meteorological Society of Japan. Ser. II, 93, 5–48, https://doi.org/10.2151/jmsj.2015-001, 2015.

Large, W. G., McWilliams, J. C., and Doney, S. C.: Oceanic vertical mixing: A review and a model with a nonlocal boundary layer parameterization, Reviews of Geophysics, 32, 363–403, https://doi.org/https://doi.org/10.1029/94RG01872, 1994.

Long, M. C., Moore, J. K., Lindsay, K., Levy, M., Doney, S. C., Luo, J. Y., Krumhardt, K. M., Letscher, R. T., Grover, M., and Sylvester, Z. T.: Simulations With the Marine Biogeochemistry Library (MARBL), Journal of Advances in Modeling Earth Systems, 13, e2021MS002 647, https://doi.org/https://doi.org/10.1029/2021MS002647, e2021MS002647 2021MS002647, 2021.

Mace, M., Fyson, C. L., Schaeffer, M., and Hare, W. L.: Large-Scale Carbon Dioxide Removal to Meet the 1.5 °C Limit: Key Governance Gaps, Challenges and Priority Responses, Global Policy, 12, 67–81, https://doi.org/https://doi.org/10.1111/1758-5899.12921, 2021.

Marshall, J., Adcroft, A., Hill, C., Perelman, L., and Heisey, C.: A finite-volume, incompressible Navier Stokes model for studies of the ocean on parallel computers, Journal of Geophysical Research: Oceans, 102, 5753–5766, 1997.

Masson-Delmotte, V., Zhai, P., Pirani, A., Connors, S., Péan, C., Berger, S., Caud, N., Chen, Y., Goldfarb, L., Gomis, M., Huang, M., Leitzell, K., Lonnoy, E., Matthews, J., Maycock, T., Waterfield, T., Yelekçi, O., Yu, R., and Zhou, B., eds.: Climate Change 2021: The Physical Science Basis. Contribution of Working Group I to the Sixth Assessment Report of the Intergovernmental Panel on Climate Change, Cambridge University Press, for the Intergovernmental Panel on Climate Change, Cambridge, 2021.

Metz, B. and Intergovernmental Panel on Climate Change, eds.: IPCC special report on carbon dioxide capture and storage, Cambridge University Press, for the Intergovernmental Panel on Climate Change, Cambridge, ISBN 9780521866439 9780521685511, oCLC: ocm64949778, 2005.

Meyer, M., Pätsch, J., Geyer, B., and Thomas, H.: Revisiting the Estimate of the North Sea Air-Sea Flux of CO2 in 2001/2002: The Dominant Role of Different Wind Data Products, Journal of Geophysical Research: Biogeosciences, 123, 1511–1525, https://doi.org/https://doi.org/10.1029/2017JG004281, 2018.

Middelburg, J. J., Soetaert, K., and Hagens, M.: Ocean Alkalinity, Buffering and Biogeochemical Processes, Rev. Geophys., 58, https://doi.org/10.1029/2019rg000681, 2020.

Oschlies, A., Stevenson, A., Bach, L., Fennel, K., Rickaby, R. E. M., Satterfield, T., Webb, R., and Gattuso, J.: Guide to Best Practices in Ocean Alkalinity Enhancement Research, State of the Planet, 2-oae2023, 3, https://doi.org/10.5194/sp-2-oae2023-3-2023, 2023.

Press, N. A.: A Research Strategy for Ocean-based Carbon Dioxide Removal and Sequestration, National Academies Press, https://doi.org/10.17226/26278, 2022.

Renforth, P.: The potential of enhanced weathering in the UK, International Journal of Greenhouse Gas Control, 10, 229–243, https://doi.org/10.1016/j.ijggc.2012.06.011, 2012.

Renforth, P. and Henderson, G.: Assessing ocean alkalinity for carbon sequestration, Reviews of Geophysics, 55, 636–674, https://doi.org/10.1002/2016rg000533, 2017.

Rickels, W., Reith, F., Keller, D., Oschlies, A., and Quaas, M. F.: Integrated Assessment of Carbon Dioxide Removal, Earth's Future, 6, 565–582, https://doi.org/https://doi.org/10.1002/2017EF000724, 2018.

Rogelj, J., Popp, A., Calvin, K. V., Luderer, G., Emmerling, J., Gernaat, D., Fujimori, S., Strefler, J., Hasegawa, T., Marangoni, G., Krey, V., Kriegler, E., Riahi, K., van Vuuren, D. P., Doelman, J., Drouet, L., Edmonds, J., Fricko, O., Harmsen, M., Havlík, P., Humpenöder, F., Stehfest, E., and Tavoni, M.: Scenarios towards limiting global mean temperature increase below 1.5 °C, Nature Climate Change, 8, 325–332, https://doi.org/10.1038/s41558-018-0091-3, 2018.

https://doi.org/10.5194/egusphere-2025-3713
Preprint. Discussion started: 27 August 2025

Subhas, A. V., Rheuban, J. E., Wang, Z. A., McCorkle, D. C., Michel, A. P. M., Marx, L., Dean, C. L., Morkeski, K., Hayden, M. G., Burkitt-Gray, M., Elder, F., Guo, Y., Kim, H. H., and Chen, K.: A tracer study for the development of in-water monitoring, reporting, and verification (MRV) of ship-based ocean alkalinity enhancement, EGUsphere, 2025, 1–34, https://doi.org/10.5194/egusphere-2025-1348, 2025.

Suselj, K., Carroll, D., Menemenlis, D., Zhang, H., Beatty, N., Savage, A., and Whitt, D.: Quantifying Regional Efficiency of Marine Carbon1 Dioxide Removal (mCDR) via Alkalinity Enhancement2 using the ECCO-Darwin Ocean Biogeochemistry State3 Estimate and an Idealized Vertical 1-D Model, Journal of Advances in Modeling Earth Systems, submitted, 123, 123–123, 2025.

Tyka, M. D.: Efficiency metrics for ocean alkalinity enhancements under responsive and prescribed atmospheric pCO_2 conditions, Biogeosciences, 22, 341–353, https://doi.org/10.5194/bg-22-341-2025, 2025.

Wang, H., Pilcher, D. J., Kearney, K. A., Cross, J. N., Shugart, O. M., Eisaman, M. D., and Carter, B. R.: Simulated Impact of Ocean Alkalinity Enhancement on Atmospheric CO2 Removal in the Bering Sea, Earth's Future, 11, e2022EF002 816, https://doi.org/https://doi.org/10.1029/2022EF002816, e2022EF002816 2022EF002816, 2023.

Wanninkhof, R.: Relationship between wind speed and gas exchange over the ocean, Journal of Geophysical Research: Oceans, 97, 7373–7382, https://doi.org/https://doi.org/10.1029/92JC00188, 1992.

Wanninkhof, R.: Relationship between wind speed and gas exchange over the ocean revisited, https://doi.org/10.4319/lom.2014.12.351, 2014.

Wanninkhof, R., Park, G.-H., Takahashi, T., Feely, R. A., Bullister, J. L., and Doney, S. C.: Changes in deep-water CO2 concentrations over the last several decades determined from discrete pCO2measurements, Deep Sea Research Part I: Oceanographic Research Papers, 74, 48–63, https://doi.org/https://doi.org/10.1016/j.dsr.2012.12.005, 2013.

Ward, N. D., Megonigal, J. P., Bond-Lamberty, B., Bailey, V. L., Butman, D., Canuel, E. A., Diefenderfer, H., Ganju, N. K., Goñi, M. A., Graham, E. B., Hopkinson, C. S., Khangaonkar, T., Langley, J. A., McDowell, N. G., Myers-Pigg, A. N., Neumann, R. B., Osburn, C. L., Price, R. M., Rowland, J., Sengupta, A., Simard, M., Thornton, P. E., Tzortziou, M., Vargas, R., Weisenhorn, P. B., and Windham-Myers, L.: Representing the function and sensitivity of coastal interfaces in Earth system models, Nature Communications, 11, 2458, 2020.

Xie, Y., Spence, P., Corney, S., Tyka, M. D., and Bach, L. T.: The effect of model resolution on air-sea CO2 equilibration timescales, Global Biogeochemical Cycles, 2025.

Yankovsky, E., Zhou, M., Tyka, M., Bachman, S., Ho, D., Karspeck, A., and Long, M.: Impulse response functions as a framework for quantifying ocean-based carbon dioxide removal, https://doi.org/10.5194/egusphere-2024-2697, 2025.

Yeager, S. G., Rosenbloom, N., Glanville, A. A., Wu, X., Simpson, I., Li, H., Molina, M. J., Krumhardt, K., Mogen, S., Lindsay, K., Lombardozzi, D., Wieder, W., Kim, W. M., Richter, J. H., Long, M., Danabasoglu, G., Bailey, D., Holland, M., Lovenduski, N., Strand, W. G., and King, T.: The Seasonal-to-Multiyear Large Ensemble (SMYLE) prediction system using the Community Earth System Model version 2, Geoscientific Model Development, 15, 6451–6493, https://doi.org/10.5194/gmd-15-6451-2022, 2022.

Zeebe, R. E. and Wolf-Gladrow, D. A.: CO2 in seawater: Equilibrium, kinetics, isotopes: Volume 65, Elsevier Oceanography Series, Elsevier Science, London, England, ISBN 9780444509468, 2001.

Zhang, H., Menemenlis, D., and Fenty, I.: ECCO LLC270 Ocean-Ice State Estimate, https://dspace.mit.edu/handle/1721.1/119821, 2018.

Zhou, M., Tyka, M. D., Ho, D. T., Yankovsky, E., Bachman, S., Nicholas, T., Karspeck, A. R., and Long, M. C.: Mapping the global variation in the efficiency of ocean alkalinity enhancement for carbon dioxide removal, Submitted to Nat. Clim. Change, 123, 123–123, 2024.